coatings

MDPI

Article

Analysis of the Interfacial Interaction between Wood Tar-Rejuvenated Asphalt and Aggregate Based on Molecular Dynamics Simulation

Le Xu [1], Guoqing Gong [2], Deliang Zeng [1], Yongwei Li [3], Xing Chen [4], Kefei Liu [1,*] and Quan Li [1,5,*]

[1] School of Civil Engineering, Central South University of Forestry & Technology, Changsha 410004, China; 20221100418@csuft.edu.cn (L.X.); 20211100402@csuft.edu.cn (D.Z.)
[2] Planning and Project Office, Department of Transportation of Hunan Province, Changsha 410004, China; ggq1998@126.com
[3] School of Civil Engineering, Central South University, Changsha 410083, China; yongweili@csu.edu.cn
[4] Hunan Expressway Engineering Consulting Co., Ltd., Changsha 410329, China; 20221200554@csuft.edu.cn
[5] Hunan Province Construction Solid Waste Resource Utilization Engineering Technology Research Center, Changsha 410083, China
* Correspondence: t20081741@csuft.edu.cn (K.L.); 20220100061@csuft.edu.cn (Q.L.)

Abstract: This study utilized molecular dynamics simulation to investigate the adhesion process between wood tar-rejuvenated asphalt and acid/alkaline aggregate. Initially, various indicators including the contact area, cohesion coefficient, and interaction energy were employed to assess the adhesion effect under dry conditions. This revealed the action mechanism of the wood tar-rejuvenator in enhancing the adhesion performance between aged asphalt and aggregate. Subsequently, an asphalt–water–aggregate interface model was developed to simulate the water damage process of the asphalt mixture. This aimed to unveil the damage mechanism of water intrusion on the adhesion performance of the asphalt–aggregate interface and evaluate the water damage resistance of wood tar-rejuvenated asphalt through adhesion energy, stripping work, and the energy ratio. The findings indicate that wood tar-rejuvenated asphalt exhibits favorable adhesion properties with both acid and alkaline aggregates. The addition of wood tar-rejuvenated asphalt increased the interaction energy between aged asphalt and acid and alkali aggregates by 67.75 kJ/mol and 97.3 kJ/mol, respectively. The addition of a wood tar rejuvenator enhances the interaction energy between aged asphalt and aggregate, thereby increasing mutual attraction and enlarging the contact area. The adhesion between asphalt and aggregates hinges on the interaction between asphaltene and aggregates, and the wood tar rejuvenator reduces the diffusion ability of asphaltene in the attractive state of the aggregate, resulting in stable aggregation. Moisture intrusion increased the aggregation distance between asphaltene and aggregate by 14.1% and decreased the degree of aggregation by 24.0%, thereby reducing the interaction energy. The extent of damage caused by water intrusion is linked to the aggregation distance, with greater distances leading to deeper damage. Under wet conditions, the interaction energy of wood tar-rejuvenated asphalt increased by 78.2% in the acidic aggregate system and 98.1% in the basic aggregate system compared with aged asphalt. Meanwhile, wood tar-based rejuvenated asphalt improves the adhesion between aged asphalt and aggregate and reduces the stripping function of asphalt affected by water replacement, which results in the ER value of wood tar-rejuvenated asphalt being higher than that of the original asphalt by 0.12 and 0.22 in the acidic and alkaline environments, respectively, thus showing excellent resistance to water damage. This study provides new criteria for the selection of rejuvenators for waste asphalt, which will help in the future selection of superior rejuvenators for aged asphalt and reduce the possibility of choosing the wrong rejuvenator.

Keywords: wood tar rejuvenator; interfacial adhesion mechanism; water damage resistance; molecular dynamics simulation

Citation: Xu, L.; Gong, G.; Zeng, D.; Li, Y.; Chen, X.; Liu, K.; Li, Q. Analysis of the Interfacial Interaction between Wood Tar-Rejuvenated Asphalt and Aggregate Based on Molecular Dynamics Simulation. *Coatings* **2024**, *14*, 905. https://doi.org/10.3390/coatings14070905

Academic Editor: Valeria Vignali

Received: 25 June 2024
Revised: 15 July 2024
Accepted: 17 July 2024
Published: 19 July 2024

1. Introduction

As a multiphase composite material commonly utilized in road construction, asphalt mixtures primarily comprise aggregates and asphalt [1]. These composite materials inherently possess interfacial bonding defects, leading to issues such as cracks, looseness, potholes, and other disorders in the early service stages of asphalt pavements [2]. Consequently, this significantly diminishes pavement performance and service life. As such, the interfacial bonding properties of asphalt and aggregate in asphalt mixtures directly dictate overall performance and durability. Moreover, asphalt pavements are continuously exposed to environmental elements, making them vulnerable to moisture damage. Prior research has demonstrated that asphalt pavements subjected to prolonged water exposure are more susceptible to asphalt–aggregate separation [3]. Additionally, the acidity or alkalinity of aggregates can influence the bonding capability of the interface [4]. Therefore, both moisture intrusion and the acidity or alkalinity of aggregates exert an impact on the overall performance of asphalt mixtures.

At present, most of the asphalt regeneration process research is focused on macro experimental research. Some microscopic test methods, such as atomic force microscopy, scanning electron microscopy, etc., can only observe the asphalt rejuvenated asphalt regeneration process of a particular moment of the microscopic state, not the entire rejuvenation of the process of change in real-time observation. The rejuvenation of asphalt in the asphalt and aggregate interfacial contact process of asphalt strength and durability is very critical. At the same time, the asphalt and aggregate interface that occurs in the ambiguity of the interaction process and leads to the rejuvenation mechanism of the rejuvenator on aged asphalt is not clear. All these aspects have led to research and development of asphalt rejuvenation performance to address the limitations, resulting in asphalt road overhaul and even reconstruction of the general situation. Molecular simulation technology using classical Newtonian mechanics solves the motion equations of microscopic molecules' trajectories to show the system's macroscopic properties and laws of motion. This is a new way to study the properties of materials, so the use of new molecular simulation technology in the rejuvenation performance research of new materials such as wood tar-rejuvenated asphalt can effectively help the recycling of asphalt. Therefore, molecular dynamics simulation can observe the miscible process of new–old asphalt in real time and probe the motion distribution of rejuvenating agents in the process of rejuvenated asphalt. In addition, through the molecular dynamics approach, the simulation technique can always calculate the magnitude and energy changes in the force between the rejuvenated asphalt and the asphalt and aggregate, thus revealing the asphalt–aggregate interfacial adhesion mechanism of wood tar-based reclaimed asphalt mixtures. Therefore, it is of great theoretical significance and practical value to conduct research on the microscopic properties of wood tar-based rejuvenated asphalt based on molecular dynamics simulation.

2. Background

Current research on the interfacial bonding of asphalt and aggregate encompasses theoretical analysis as well as experimental investigation. In terms of theoretical analysis, Li et al. [5] proposed an evaluation index for the self-healing performance of asphalt mixtures based on the integral principle of fracture mechanics. Their research revealed that more cycles of damage healing resulted in a closer approximation of the crack curve to linear development. Bagampadde et al. [6] proposed an evaluation index for the self-healing performance of asphalt mixtures based on the integral principle of fracture mechanics. Their research revealed that more cycles of damage healing resulted in a closer approximation of the crack curve to linear development. This enabled the construction of a calculation formula for the self-healing performance of asphalt mixtures and pavement. Yalghouzaghaj et al. [7] employed thermodynamic theory and surface free energy theory to examine the effect of material basic properties on the debonding effect of the asphalt–aggregate interface at low-temperature conditions. Their findings indicated that higher bonding free energy can enhance the low-temperature strength of asphalt mixtures and improve adhesion

between asphalt and aggregates. Sun et al. [8] used surface structure theory combined with hierarchical prediction methods to analyze the impact of the microstructure of coarse aggregate on the bonding capacity of the asphalt–aggregate interface in asphalt mixtures. They found that the Mori–Tanaka model they constructed could be utilized to analyze the thermal shrinkage strain of asphalt mixtures. Regarding experimental studies, scanning electron microscopy (SEM) [9], dynamic shear rheometer (DSR) [10], X-ray computed tomography (CT) [11], atomic force microscopy (AFM) [12], and the dynamic mechanical analyzer (DMA) [13] are commonly employed to explore the interfacial adhesion mechanism of asphalt mixtures. Although these theoretical analyses and experimental methods have achieved effective results to a certain extent, mixtures are often regarded as continuous wholes rather than multiple composite materials. Given that the bonding properties of asphalt mixture are inherently multiscale, their bonding effect varies because of the influence of material properties at different spatial and temporal scales [14]. Furthermore, current explorations of the bonding mechanism of asphalt mixtures are typically confined to phenomenological descriptions of the macroscopic behavior of materials, disregarding the potential mechanism of bonding at the asphalt–aggregate interface [15].

On the other hand, there is a significant number of asphalt pavements worldwide that require major repairs or even reconstruction, resulting in a substantial amount of waste asphalt produced annually [16]. The accumulation of this waste not only wastes space resources but also pollutes the environment, making it imperative to implement waste asphalt regeneration [17,18]. The research and development of rejuvenators based on biomass materials has garnered widespread attention in recent years because of their ecological and environmental friendliness and the broad range of materials available. However, wood tar, as a biomass oil, has not received sufficient attention. Wood tar can be produced from bamboo or wood through high-temperature cracking or hydrothermal liquefaction, and it possesses a wide range of sources, as well as environmentally friendly and renewable characteristics. It contains a significant amount of lightweight aromatic components, making it suitable as a substrate for the preparation of aged asphalt rejuvenators [19].

In recent years, molecular dynamics (MD) simulation has gained increasing attention because of its superior microscale analysis capability. The MD method enables the analysis of complex thermodynamic properties of non-homogeneous systems by directly describing the atomic behavior of a material without the need for predefined material parameters [20] while considering the impact of changes in molecular structure [21]. Consequently, MD simulation has emerged as a potent tool for studying the interfacial bonding properties of asphalt mixtures. Xu et al. [22] examined the influence of water on the adhesion ability of the asphalt–aggregate interface at various aging levels using the MD method. Their findings revealed that aging enhances the adhesion effect of asphalt–aggregate in asphalt mixtures, which is influenced by the presence of water. Moreover, modifiers can also affect the interfacial adhesion effect of asphalt–aggregate. Yao et al. [23] investigated the impact of nano-hydrated lime (NHL) on the water sensitivity of asphalt mixtures through MD simulations, demonstrating that NHL enhances the adhesion ability of the asphalt-aggregate interface in wet environments. Similarly, silane coupling agents [24] and styrene–butadiene–styrene (SBS) [25] have been validated through MD simulation for their role in enhancing the bonding effect at the asphalt–aggregate interface. Liu et al. [26] developed a novel asphalt mixture by substituting aggregate with waste steel slag, and MD simulations were employed to simulate asphalt aggregation on steel slag under dry and wet conditions. Their results indicated that asphalt exhibits a higher tendency to form adhesion with alkaline steel slag, with temperature and humidity being key factors influencing overall asphalt mixture performance. Gong et al. [27] utilized MD to investigate the effect of moisture on the interaction between asphalt and aggregate at varying temperatures, revealing that temperatures exceeding the softening point of asphalt can exacerbate the moisture-induced weakening effect on bonding properties. Zheng et al. [28] employed MD to explore the influence of asphalt component ratio characteristics on microscopic adhesion effects at the aggregate–asphalt interface in cold regions. Their results highlighted

that the adhesion effect of asphalt–aggregate is primarily determined by the attraction of saturates and aromatics to the mineral surface at low temperatures. Furthermore, Zhou et al. [29] studied the impact of humidity and water pressure on the adhesion effect at the asphalt–aggregate interface through MD simulations, indicating that surface water pressure has a more pronounced effect on reducing adhesion ability than humidity. Moreover, the anisotropy and acid–alkalinity of aggregate also influence the interfacial adhesion effect [30]. While it is feasible to employ MD simulation to investigate the adhesion ability between asphalt and aggregate, most of the current research is focused on modified asphalt mixtures, with relatively limited exploration of the water stability performance of rejuvenated asphalt mixtures. The exploration of the action mechanism for the impact of biomass rejuvenators such as wood tar on the adhesion of the aged asphalt–aggregate interface is still in its early stages, and there is an urgent need for an in-depth and systematic study to be carried out.

To elucidate the adhesion mechanism of the asphalt–aggregate interface in wood tar-rejuvenated asphalt mixtures, MD simulation was employed to investigate the adhesion effect of wood tar-rejuvenated asphalt with acidic/alkaline aggregates under dry and wet conditions. An extracted oil rejuvenator was designated as the control group to quantitatively assess the adhesion effect of wood tar-rejuvenated asphalt using relevant indicators. Ultimately, this study unveiled the mechanism of water damage in rejuvenated asphalt and the adhesion mechanism through which the wood tar rejuvenator enhances the adhesion effect between aged asphalt and aggregate.

3. Molecular Dynamics Modeling and Validation

In this study, the three-dimensional materials science simulation software Materials Studio 2023 developed by Accelrys Company was used for the simulation, the force field was the COMPASS II force field adapted to the complex molecular environment, and the boundary conditions were set to be periodic, which can eliminate the influence of the boundary between asphalt molecules. In order to simulate the process of asphalt molecules miscible with each other efficiently, the temperature was controlled by the Nose–Hoover method and the pressure was controlled by the Andersen method. The truncation distance in this paper was set at 15.5 Å, the van der Waals non-bonding effect was calculated by the Atom-based method, and the electrostatic non-bonding effect was calculated by the Ewald method to make sure that the accuracy of the simulation experiments met the minimum demand of model iteration. The modeling process used the Amorphous Cell module to build the corresponding molecular model; the initial density was set to 0.1 g/cm^3 to ensure the random distribution of molecules and then the molecules were mixed within the original asphalt model sufficiently by using the NVT system at 300 ps (with the number of particles in the system (N), the volume (V), and the temperature (T) kept constant). Then, a 500 ps simulation was performed in the NPT system (with the number of particles in the system (N), pressure (P), and temperature (T) kept constant) for 500 ps to make the system shrink in volume until the cell dimensions were stable and the change in each time step was small. In order to minimize the total energy of the molecular structure of the asphalt, geometry optimization iterations were performed using the Forcite module for 20,000 steps with the default accuracy set to Fine and constant convergence through the iterations to ensure the correctness of the structure. Finally, different asphalt models were built. The simulation flow is shown in Figure 1.

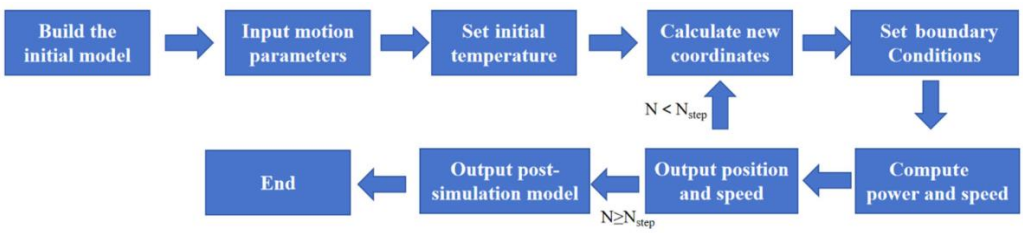

Figure 1. MD simulation flowchart.

3.1. Construction of the Asphalt Molecular Model

This study utilized the Amorphous Cell module in the three-dimensional material science simulation software Materials Studio to create an asphalt molecular model. Employing the component classification method that closely resembles actual asphalt composition, the molecular structure model of asphalt was developed using the following four components: asphaltene (As), resin (R), saturate (S), and aromatic (Ar).

Su et al. [31] constructed a model of asphaltene components that was verified by experiments documented in the literature such as nuclear magnetic resonance (NMR) analysis, quantum chemical methods, X-ray scattering techniques, small angle analysis, etc. Asphaltene contains a small number of short, branched chains with a moderately sized aromatic ring [32]; therefore, in this paper, we selected the molecule shown in Figure 2a as a representative molecule of asphaltene. Resins are layered structural fractions composed of thick cyclic aromatic hydrocarbons and alicyclic hydrocarbons [33]; so, in this paper, the molecule shown in Figure 2c was selected as a representative molecule of asphalt resin. The chain lengths of alkane molecules in bitumen are distributed between C16 and C36, where C22 is just distributed in the middle part of this region. Bitumen contains the highest content of C22H46 among alkanes and, at the same time, the softening and boiling points of C22H46 are consistent with those of the majority of the oils in bitumen [34]. Therefore, in this paper, the molecule shown in Figure 2e was selected to be the saturated fraction representative molecule. In addition, the number of aromatic rings and the number of straight chains in the molecular structure of 1,7-dimethylnaphthalene are similar to the number of aromatic fractions of asphalt [35]; therefore, the molecule shown in Figure 2f was selected to represent the aromatic fraction molecule in this paper. Additionally, based on the study of the aging mechanism of asphalt caused by oxidation [36,37], ketone and sulfoxide were identified as typical functional groups formed after asphalt oxidation. Long-term oxidative aging (PAV) can be characterized by adding these functional groups to the oxidation-prone sites of asphaltene and resin models. For instance, ketone is formed by replacing the hydrogen atom originally attached to the benzyl carbon (the first carbon connected to the aromatic ring) with an oxide, and sulfoxide is formed by adding an oxide to the oxidation-prone sulfur atom. The models of PAV-aged asphaltene and aged resin are depicted in Figure 2b,d. In summary, the four-component molecular model of asphalt was established in Materials Studio software, as illustrated in Figure 2.

This study employed original 70# matrix petroleum asphalt as the control group and conducted a component analysis of the original asphalt before and after PAV aging according to the method specified in T0618-1993 in the Chinese specification JTG E20-2011 [38]. The results are presented in Table 1.

Table 1. Component analysis results of each asphalt.

Asphalt Type	Penetration/(25 °C, 0.1 mm)	Softening Point/°C	Ductility /(10 °C, cm)	Viscosity /(135 °C, Pa·s)	w(As) /%	w (R)/%	w(S) /%	w(Ar) /%
Original 70# matrix asphalt	63.2	47.5	25.3	0.34	10.34	25.85	14.88	48.93
PAV-aged 70# matrix asphalt					16.75	30.16	14.47	38.62

Based on the mass ratio among the components in Table 1, the quantity ratio was calculated from the molecular formula of each component, resulting in As:R:S:Ar = 4:7:17:113 for the original asphalt and As:R:S:Ar = 7:9:19:103 for the PAV-aged asphalt. The Amorphous Cell module was utilized to construct the corresponding molecular model, with the initial density set at 0.1 g/cm^3 to ensure the random distribution of molecules. Subsequently, a 300 ps NVT system (with the number of particles (N), volume (V), and temperature (T) in the system unchanged) was employed to thoroughly mix the molecules in the original asphalt model. This was followed by the use of a 500 ps NPT system (with the number of

particles (N), pressure (P), and temperature (T) in the system unchanged) to reduce the volume of the system until the crystal cell size stabilized with minimal change at each time step. To minimize the total energy of the asphalt molecular structure, the Forcite module was utilized for 20,000 steps of geometric optimization iterations, with the default accuracy set to Fine. The iterative convergence was continued to ensure the correctness of the structure, ultimately yielding the models of the original (VB) and PAV-aged 70# matrix asphalt (PB), as depicted in Figure 3a,b.

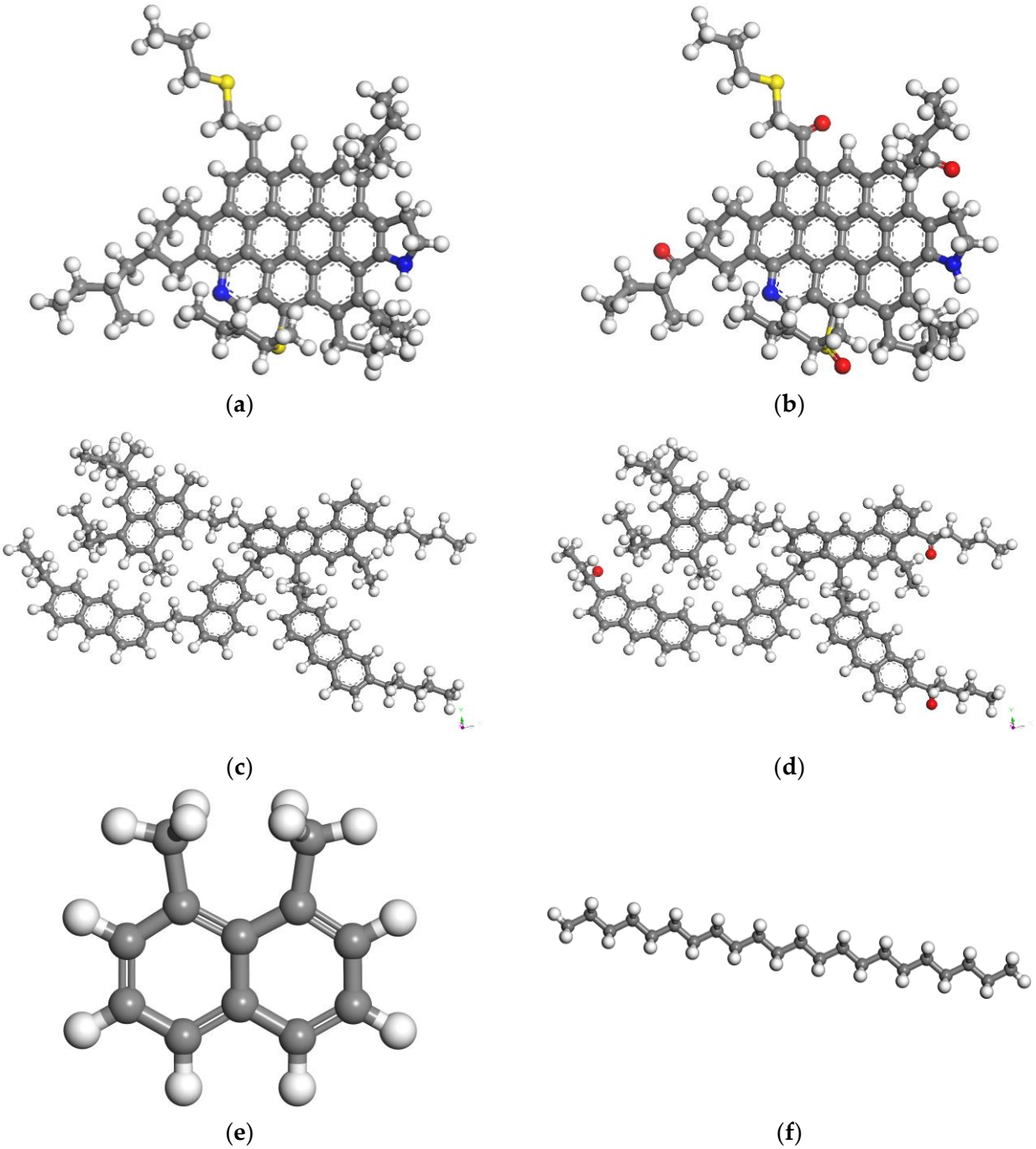

Figure 2. Molecular simulation of asphalt components (note: gray represents a carbon atom, white represents a hydrogen atom, blue represents a nitrogen atom, yellow represents a sulfur atom, and red represents an oxygen atom). (**a**) Asphaltene; (**b**) PAV-aged asphaltene; (**c**) resin; (**d**) PAV-aged resin; (**e**) saturate; and (**f**) aromatic.

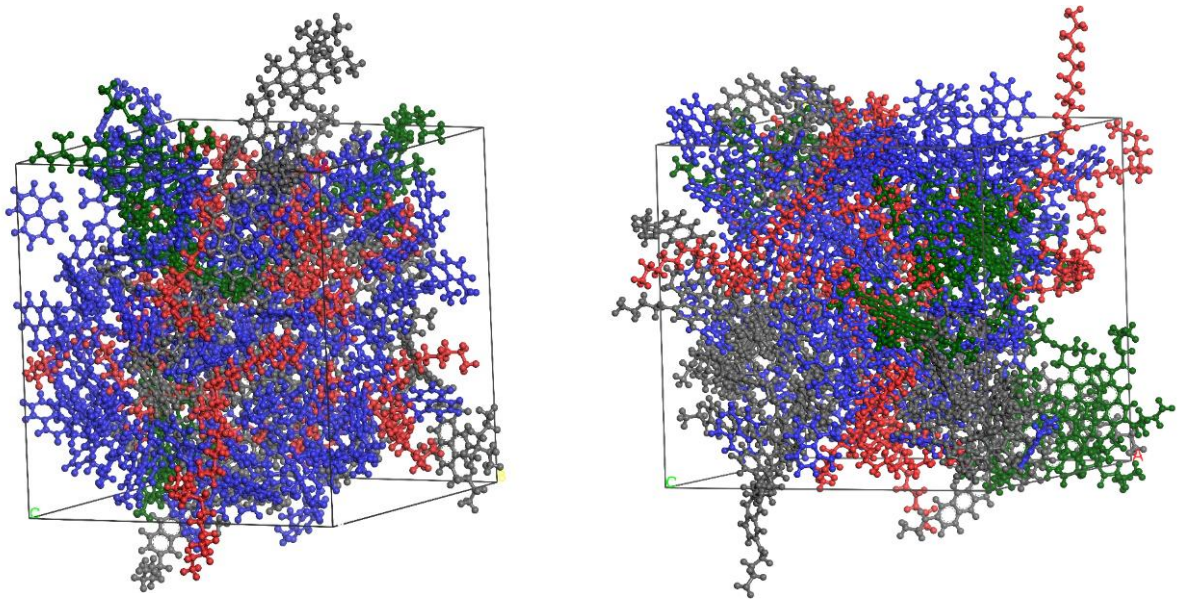

(**a**) (**b**)

Figure 3. Molecular model of asphalt (note: red represents saturate, blue represents aromatic, green represents asphaltene, and grey represents resin). (**a**) Original 70# matrix asphalt; (**b**) PAV-aged 70# matrix asphalt.

3.2. Construction of the Rejuvenated Asphalt Molecular Model

In this study, wood tar was utilized as the base material to formulate the aged asphalt rejuvenator. Wood tar is the high-temperature pyrolysis product of woody biomass materials, which can be derived from waste wood and bamboo. It is characterized by its wide availability, economic viability, and environmental friendliness. Wood tar is an organic compound with high concentrations of alcohols, acids, and phenols [39]. Because of its complex composition, the main molecular structures with relatively high contents were selected when constructing the molecular model of wood tar. Research has indicated [40] that bamboo-based wood tar primarily comprises tetracosanoic acid, guaiacol, syringol, and phenolic aldehyde, with a mass ratio of 47:19:23:11 and a density of 1.15 g/cm^3. Its basic properties are shown in Table 2. It is worth noting that, unlike the simulations in this article, wood tar in real environments has a certain degree of corrosiveness and permeable fume odor, which requires attention to protection in actual use. For comparative purposes, the extracted oil, refined by petroleum distillate solvent and desolvent treatment, was utilized as the control group. This oil mainly consists of saturated alkanes, cycloalkanes, and aromatic hydrocarbons [41], with a mass ratio of 53:31:16 and a density of 0.92 g/cm^3. By inputting the above component composition and density into the software, the final molecular models of the two rejuvenators were obtained, as shown in Figure 4.

The asphalt rejuvenation process involves the blending of original asphalt and aged asphalt with a rejuvenator to create a new rejuvenated asphalt with stable properties. Based on the original and aged asphalt model and rejuvenator model established in the previous section, rejuvenated asphalt is modeled in this section. The Amorphous Cell function was employed to construct a model of rejuvenated asphalt without a rejuvenator using a 1:1 molar ratio of the original matrix asphalt to aged asphalt. The initial density was set to 0.1 g/cm^3 to ensure the random distribution of asphalt component molecules within the crystal cell, and the system energy was stabilized through 20,000 steps of geometric optimization. Subsequently, the rejuvenated asphalt was uniformly stirred by relaxation of the NVT system, followed by the formation of a stable asphalt model through relaxation and compression of the NPT system. Furthermore, the extracted oil-rejuvenated asphalt model (EA) with a 15% mass ratio of rejuvenator addition and the wood tar rejuvenator-

rejuvenated asphalt model (WA) were also built as described above. Each model is depicted in Figure 5.

Table 2. Basic properties of wood tar.

Item	Viscosity/ (60 °C, Pa·s)	Flashing Point/°C	Content of Saturate/%	Content of Aromatic/%	Viscosity Ratio before and after RTFOT	Mass Change before and after RTFOT/%
Wood tar	5820	298	18.7	59.6	1.4	0.25

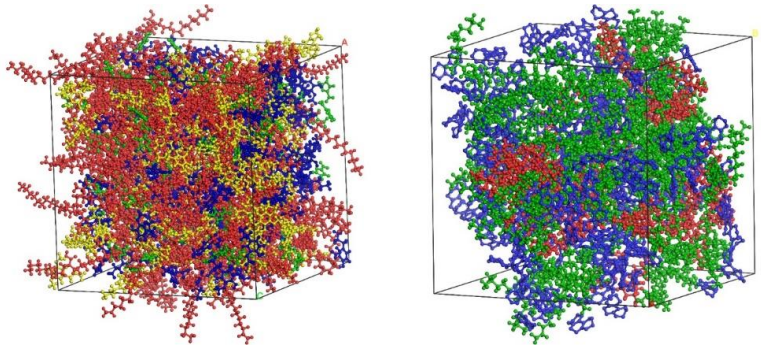

(**a**) (**b**)

Figure 4. Molecular models of rejuvenators (note: in (**a**), red represents tetracosanoic acid, blue represents guaiacol, yellow represents syringol, and green represents phenolic; in (**b**), red represents cycloalkane, blue represents aromatic hydrocarbon, and green represents saturated hydrocarbon). (**a**) Wood tar molecule; (**b**) extracted oil molecule.

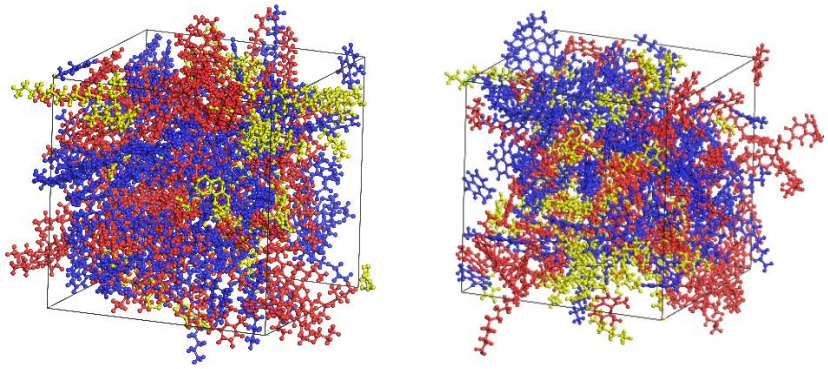

(**a**) (**b**)

Figure 5. Molecular model of each rejuvenated asphalt (note: blue represents original asphalt, red represents aged asphalt, and yellow represents rejuvenator). (**a**) Extracted oil-rejuvenated asphalt; (**b**) wood tar-rejuvenated asphalt.

3.3. Construction of the Aggregate Molecular Model

Aggregates in asphalt mixtures are taken from a wide variety of materials, and different mineral compositions can lead to significant differences in their physical and chemical properties. It has been shown that the acidity or alkalinity of the aggregate is a key factor affecting its adhesion properties to asphalt [42]. For example, acidic aggregate quartz, primarily composed of silica, and alkaline aggregate calcite, mainly consisting of calcium carbonate, exhibit contrasting properties. In order to investigate the influence of aggregate properties on asphalt–aggregate inter-adhesion properties, quartz crystals and calcite crystals from the Cambridge Crystal Structure Database (CSD) were selected in this study to represent acidic and alkaline aggregates, respectively, with the modeling units illustrated in Figure 6. The lattice parameters of the two minerals are detailed in Table 3.

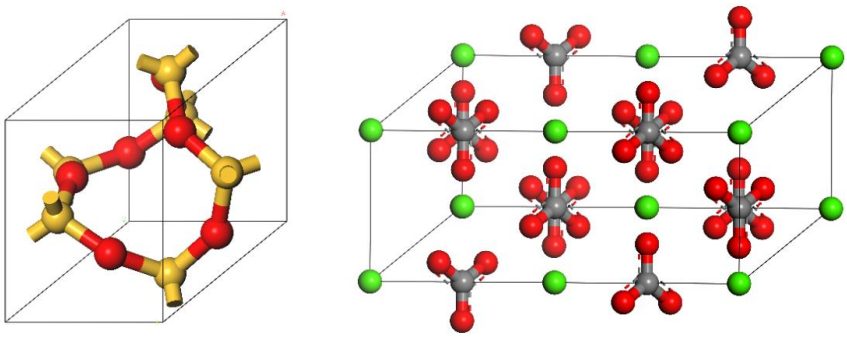

(**a**) (**b**)

Figure 6. Aggregate model unit. (**a**) Quartz; (**b**) calcite.

Table 3. Lattice parameters of the two aggregates.

Aggregate Type	Crystal System	Space Group	Lattice Parameter	Coordination Number
Quartz	tripartite crystal system	P3221	a = b = 4.91 Å c = 5.402 Å α = β = 90° γ = 120°	Si-O: 4 Si-O: 4
Calcite	tripartite crystal system	R-3C	a = b = 4.988 Å c = 17.061 Å α = β = 90° γ = 120°	Ca^{2+}-CO_3^{2-}: 6 C-O: 3

Aggregates in asphalt mixtures are typically mechanically processed to create crushed surfaces, with the aggregates tending to break along surfaces with weak interatomic bond strengths. Therefore, in this study, the quartz {0 0 1} surface and the calcite {1 0 4} surface, as commonly exposed surfaces [30], were selected. The crystals tool was utilized to build the cellular structure and incorporate three-dimensional periodic boundaries, while the supercell tool was employed to construct the supercell structure. This was performed to ensure that the aggregate cellular parameter closely approximated the cellular parameter of the asphalt molecule. The aggregate model is depicted in Figure 7.

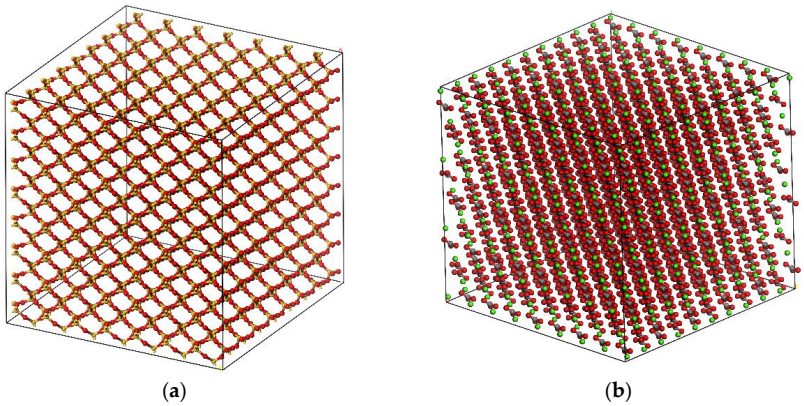

(**a**) (**b**)

Figure 7. Aggregate molecular model. (**a**) Supercell structure of quartz. (**b**) Supercell structure of calcite.

4. Effect of the Asphalt–Aggregate Interface Interaction

An asphalt mixture is a multiphase composite material consisting of aggregate and asphalt, and the interaction surface between the two components is crucial to its overall performance. The occurrence of pavement distress such as rutting, fatigue cracking, and water damage in the normal course of use is related to the properties of this interface. Because of the limitations of current macroscopic methods in clearly representing the

interaction process at the asphalt–aggregate interface, molecular dynamics simulations were employed to analyze the adhesion properties at this interface.

4.1. Construction of the Asphalt–Aggregate Interface Model

Utilizing the previously established asphalt and aggregate models, the asphalt and aggregate layers were overlaid using the build layers module. Additionally, a vacuum layer with a thickness of 60 Å was added to the upper layer to mitigate the adverse effects of the remaining periodic models in the *Z*-axis direction on the asphalt arising from the three-dimensional periodic boundary conditions. Furthermore, to minimize experimental errors, the aggregate was entirely fixed, ensuring that it would not be displaced during the simulation. The constructed model underwent geometric optimization to eliminate any irregularities, and subsequently, the NVT system was relaxed over 500 ps. The simulations were conducted at 298 K, with a time step of 1 fs and a truncation radius of 15.5 Å. Each asphalt–aggregate interface model is depicted in Figure 8. To simplify expression, the Original 70# matrix asphalt is abbreviated as VA, the PAV-aged 70# matrix asphalt is abbreviated as PA, the extracted oil-rejuvenated asphalt is abbreviated as EA, and the wood tar-rejuvenated asphalt is abbreviated as WA.

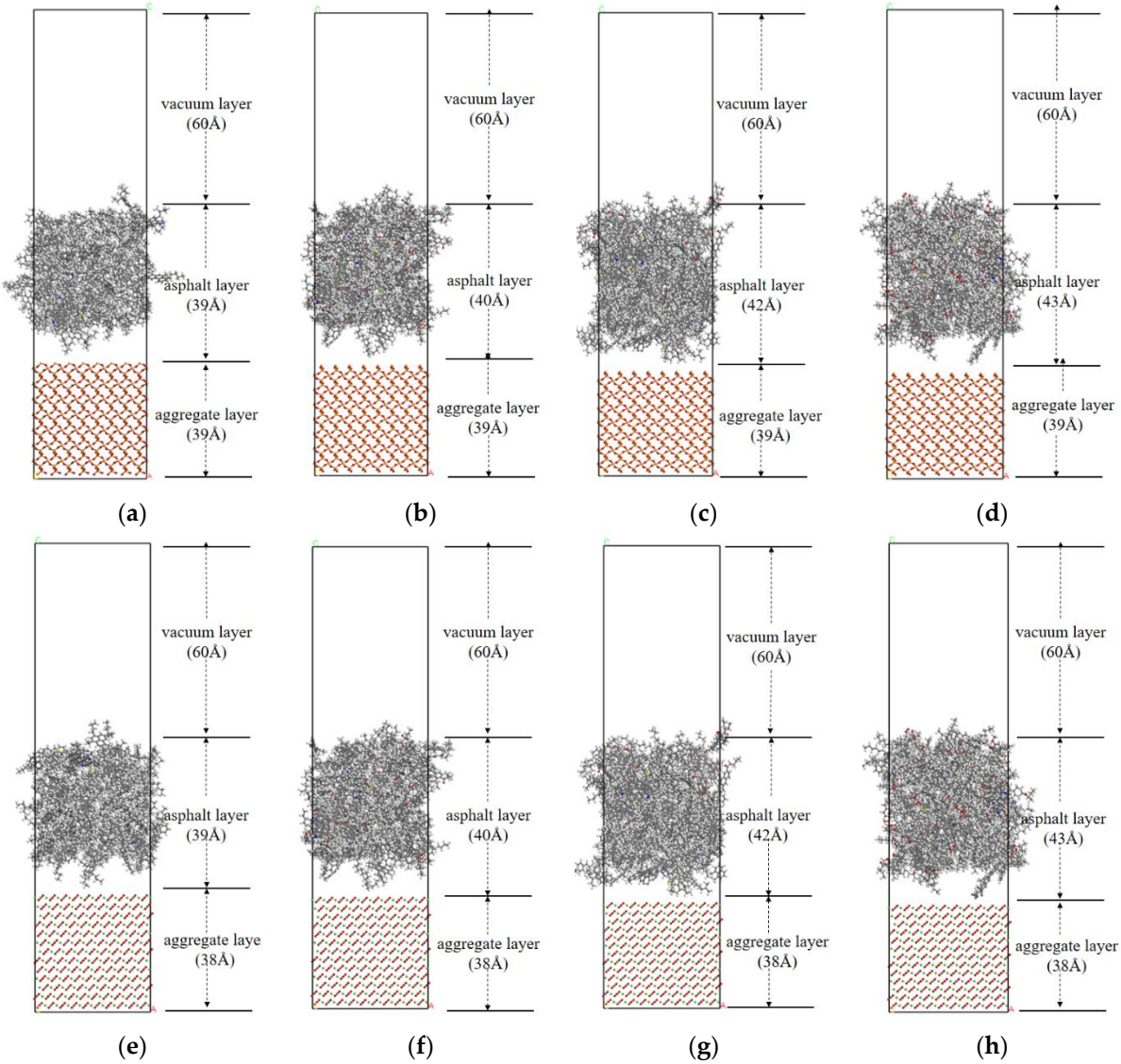

Figure 8. Asphalt–aggregate interface modeling diagram. (**a**) VA–quartz; (**b**) PA–quartz; (**c**) EA–quartz; (**d**) WA–quartz; (**e**) VA–calcite; (**f**) PA–calcite; (**g**) EA–calcite; and (**h**) WA–calcite.

4.2. Diffusion Analysis during the Interaction Process between Asphalt and Aggregate

4.2.1. Relative Concentration Analysis

Relative concentration is defined as the ratio of the number of atoms in a unit volume perpendicular to the axis direction to the average number of atoms per unit volume relative to the total volume. It is calculated as shown in Equations (1) and (2).

$$c_i = N_i / V_i \tag{1}$$

$$RC_i = c_i / c_{bulk} \tag{2}$$

where c_i and c_{bulk} are the concentrations (mol/L) of the incubated slab i and the whole cell, respectively, N_i is the number of molecules in the slab (mol), V_i is the volume of the slab (cm^3), and RC_i is the corresponding relative concentration.

Relative concentrations were employed to analyze the distribution of asphalt molecules along the *Z*-axis direction. The model was segmented into an infinite number of unit volume spaces along the *Z*-axis direction (i.e., the long side of the interface model), and the relative concentrations were computed. The trajectory files obtained after the relaxation of the NVT system were inputted into Equations (1) and (2), and the concentration distribution curves along the *Z*-axis were calculated using the Analysis function, as illustrated in Figures 9 and 10.

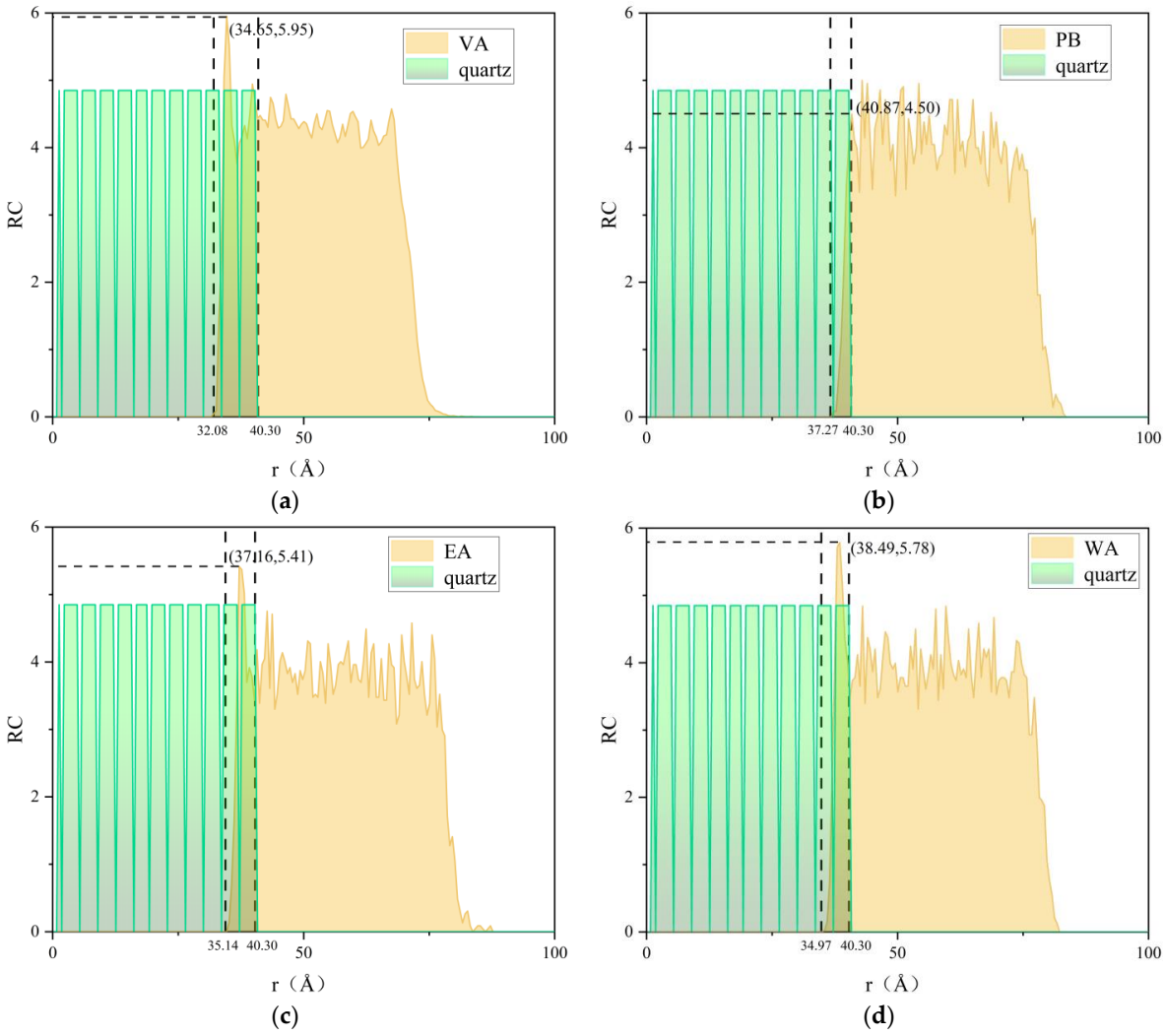

Figure 9. Relative concentration analysis plots for each asphalt–quartz interfacial model. (**a**) VA–quartz; (**b**) PA–quartz; (**c**) EA–quartz; and (**d**) WA–quartz.

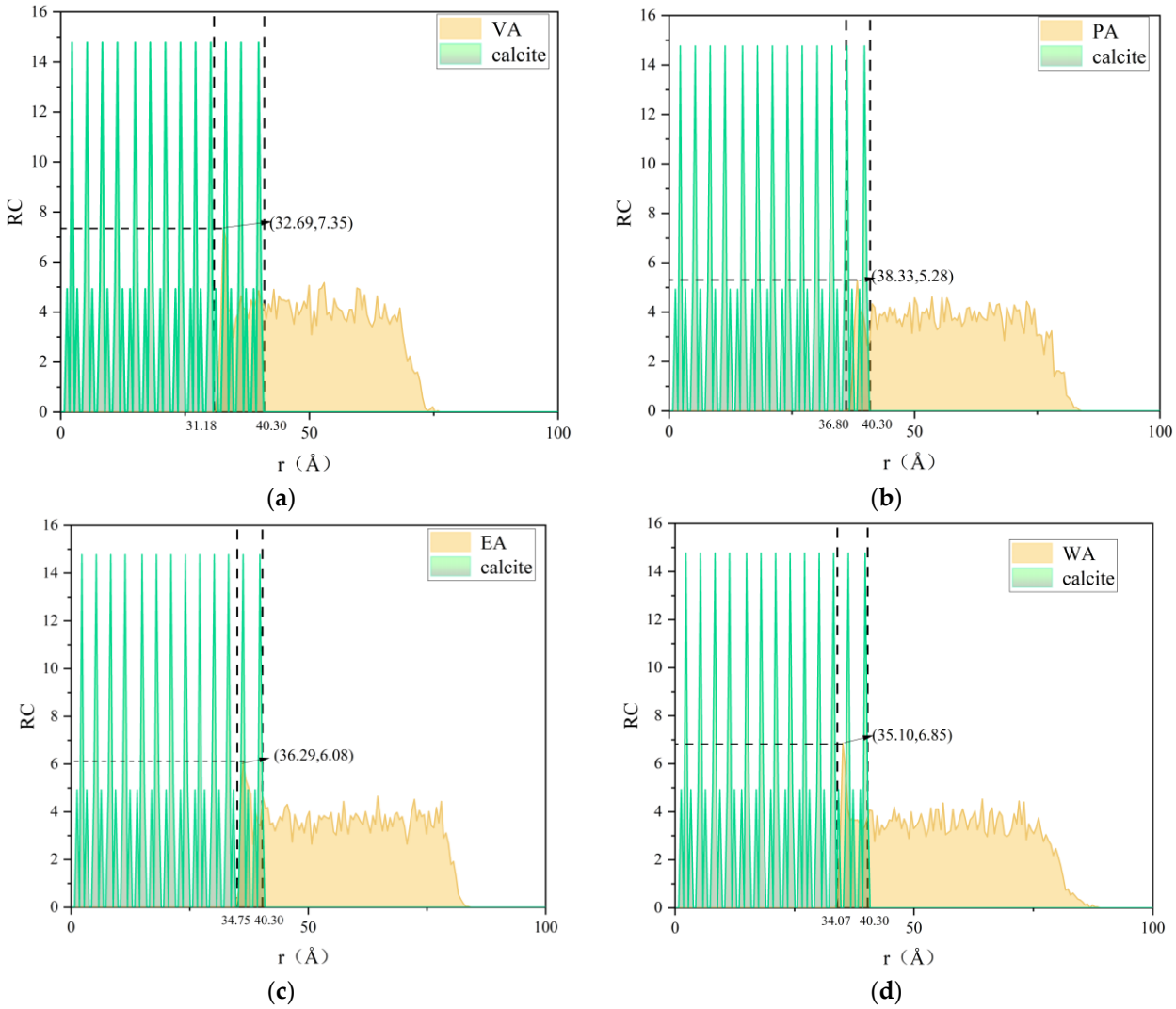

Figure 10. Relative concentration analysis plots for each asphalt–calcite interface model. (**a**) VA–calcite; (**b**) PA–calcite; (**c**) EA–calcite; and (**d**) WA–calcite.

As shown in Figures 8 and 9, both aggregates are uniformly distributed in the region of 0 Å to 40.30 Å along the *Z*-axis. This can be attributed to the fixed positioning of the aggregates in the interface model, preventing displacement during the relaxation process. This characteristic facilitates a more intuitive analysis of the asphalt concentration distribution after relaxation under the influence of the aggregates. Furthermore, the presence of peaks on both sides of the asphalt near the aggregate suggests that the aggregate's attraction impacts the distribution of asphalt molecules. Upon comparison of Figure 9 with Figure 10, it is evident that the peak of asphalt near the calcite side is slightly larger than that near the quartz side, indicating that alkaline aggregates exhibit a stronger attraction to asphalt than acidic aggregates. Additionally, the aging asphalt demonstrates smaller peaks compared with the virgin asphalt, signifying that aging makes the interaction between asphalt and aggregate less effective, resulting in slower movement of internal molecules towards the aggregate side. Moreover, the rejuvenator significantly enhances the peak value of asphalt near the aggregate side, with the wood tar-rejuvenated asphalt exhibiting a more pronounced effect compared with the extracted oil-reclaimed asphalt, indicating superior adhesion of the wood tar-rejuvenated asphalt to the aggregate.

Prior to relaxation, no contact between asphalt and aggregate is observed. However, in both Figures 8 and 9, some contact between asphalt and molecules on the surface of the aggregate can be seen, indicating a close proximity between asphalt and aggregate during

the contact process. The range between the two dashed lines in the figures represents the transition zone between the asphalt layer and the aggregate layer along the *Z*-axis. A larger transition zone indicates closer contact between the two. In Figure 8, the transition zone ranges in descending order are VA (8.28 Å) > WA (5.33 Å) > EA (5.16 Å) > PA (3.03 Å). In Figure 9, the transition zone ranges in descending order are VA (9.12 Å) > WA (6.23 Å) > EA (5.55 Å) > PA (3.5 Å). The ordering of contact range sizes for the two aggregate interface models is consistent, with the combination of the virgin asphalt and each aggregate exhibiting the closest contact. Additionally, the transition zone range of the PAV-aged asphalt is only about two-fifths of that of the virgin asphalt, explaining the susceptibility of aggregates to detachment from aged asphalt mixtures [43]. The transition zone range of the reclaimed asphalt is greater than that of the PAV-aged asphalt, indicating that the rejuvenator enhances the contact between aged asphalt and aggregates. Furthermore, the wood tar rejuvenator performs slightly better than the extracted oil rejuvenator in promoting aggregate–asphalt contact. Comparing the contact ranges at the quartz and calcite interfaces, it is observed that the contact range of alkaline aggregates with asphalt is larger than that of the corresponding acidic aggregates. This suggests that alkaline aggregates exhibit a stronger attraction to asphalt compared with acidic aggregates, aligning with the conclusion drawn from the aforementioned peak phenomenon of asphalt molecules near the aggregates.

4.2.2. Diffusion Coefficient Analysis

The diffusion coefficient represents the average rate at which molecules pass through a unit area under the influence of a concentration gradient. To calculate the mean square displacement (Å2) of the molecules in the model system, the Einstein equation was employed, resulting in the MSD curve. The MSD curve illustrates the changes in molecular displacements over time during molecular motion, and it is calculated using Equations (3) and (4).

$$MSD(t) = \left\langle |r_i(t) - r_i(0)|^2 \right\rangle \tag{3}$$

$$D = \frac{1}{6N} \lim_{t \to \infty} \frac{d}{dt} \sum_{i=1}^{N} \left\langle |r_i(t) - r_i(0)|^2 \right\rangle \tag{4}$$

where $r_i(0)$ is the initial position of the center of mass of atom i, $r_i(t)$ is the position of the center of mass of atom i at time t, D is the diffusion coefficient of particles in the model system (m^2/s), and N is the number of molecules diffusing in the system (mol). The differential term denotes the linear slope of the mean-square displacement with respect to time, and the angular brackets denote an overall average of all the atoms and all the simulation times.

Since the number of molecules (N) in the system is fixed, the obtained diffusion coefficient (D) is proportional to the mean square displacement (MSD). Therefore, Equation (4) can be approximated and simplified to Equation (5) when the linear relationship between the mean square displacement and time is favorable.

$$D = \frac{a}{6} \tag{5}$$

where a is the linear slope of the mean square displacement versus time.

Calculations were performed using the Forcite Analysis module to obtain a series of trajectory files, reflecting the positional data of the molecules in the rejuvenated asphalt system over time. Based on these trajectory files, the mean square displacement values of the system were analyzed. Each component of asphalt in the interface model was selected as a representative substance for this study. Two methods were employed to ensure that the mean square displacement maintained a good linear relationship with time during the calculation process. First, the simulation time period during which the energy and density of the system changed significantly in the early stages of relaxation when the system had

not yet reached equilibrium, was excluded, selecting the equilibrium state as the study period. Second, molecular trajectories were screened for Brownian motion consistent with Einstein's theory [44], selecting portions of the curves with a slope of 1 through log-mean-square displacement and log-time to exclude molecules subjected to anomalous diffusion due to the diversity of molecules in the asphalt and the model's complexity. The MSD-fitted curves were obtained by linear fitting using Origin 9.1 software to characterize the diffusion coefficients. The MSD curve fitting results for each component of asphalt are shown in Figures 11 and 12.

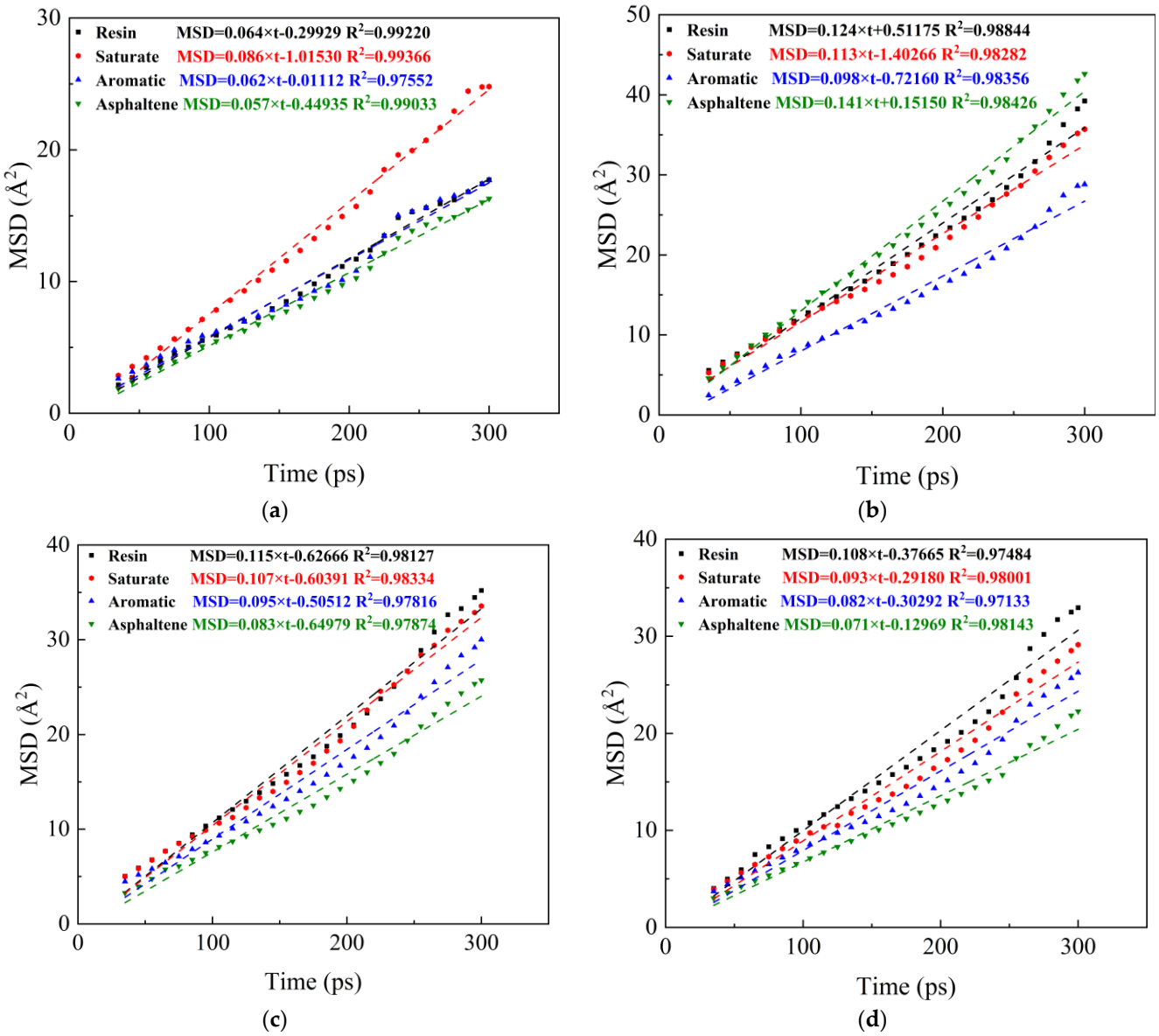

Figure 11. Mean square displacement curves of asphalt components in the quartz interface. (**a**) VA–quartz; (**b**) PA–quartz; (**c**) EA–quartz; and (**d**) WA–quartz.

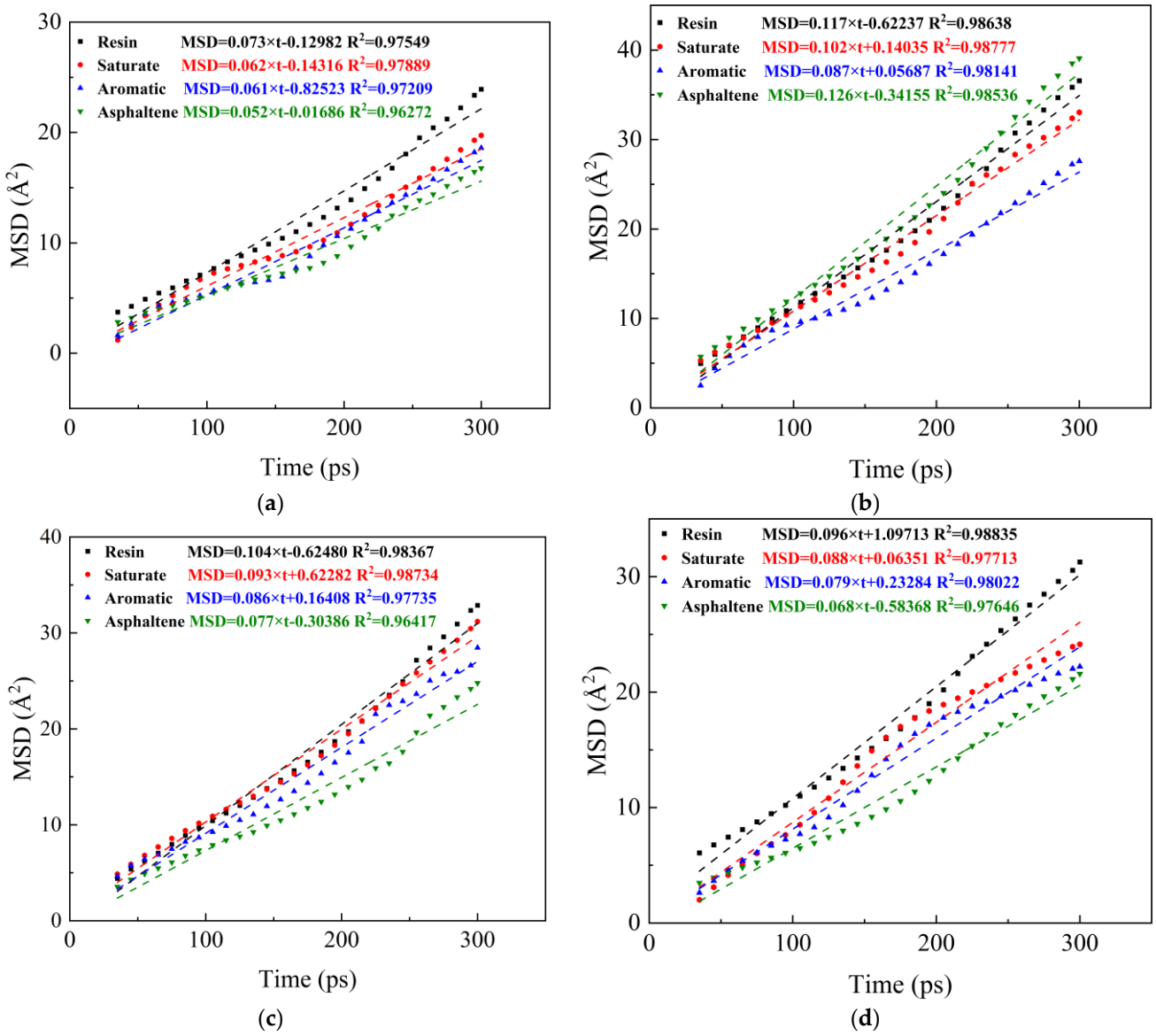

Figure 12. Mean square displacement curves of asphalt components in the calcite interface. (**a**) VA–calcite; (**b**) PA–calcite; (**c**) EA–calcite; and (**d**) WA–calcite.

As observed in Figures 10 and 11, the MSD values of each component of asphalt exhibit an approximately linear increase with simulation time, displaying different growth patterns in different aggregate models. A higher MSD value indicates a greater distance covered by the component in the same amount of time, indicating stronger diffusion ability. However, the attraction exerted by the aggregates inhibits the diffusion of asphalt, confining it to the area adjacent to the aggregates. Therefore, a lower MSD value indicates a higher degree of adsorption and stronger interaction between asphalt and aggregates, while a higher MSD value suggests a lower degree of adsorption and weaker mutual attraction with aggregates.

At the quartz interface, the MSD values of each component of the virgin asphalt at 300 ps in descending order are saturate > resin > aromatic > asphaltene. This indicates that asphaltene moves the slowest and has the strongest adsorption with quartz, with its molecules slowly approaching and distributing at the quartz interface over time. Aromatic, as a light component, typically would have the highest MSD value in undisturbed conditions, but under quartz's attraction, it shows a low MSD value, second only to asphaltene. This suggests that, among the virgin asphalt components, aromatic and asphaltene are most closely connected to quartz, with the weakest interaction between resin and quartz.

Similarly, the MSD values of each component of the PAV-aged asphalt in descending order are asphaltene > resin > saturate > aromatic. Compared with the original asphalt, the aged asphaltene shows the largest MSD value, indicating that it is less attracted to quartz, possibly because ketone and sulfoxide groups reduce the energy difference between aged asphaltene and quartz [25]. Resin molecules in the aged asphalt are also affected, with MSD values only second to asphaltene, and both components showing higher MSD values than their counterparts in the virgin asphalt. This indicates that aging negatively impacts the bonding process between asphalt and aggregate, suggesting that relying solely on lightweight components such as aromatic and saturates to connect asphalt to aggregate is unreliable and leads to the separation of the asphalt system from the aggregate. Comparing Figure 10c,d, the MSD values of each component in the two types of rejuvenated asphalt in descending order are resin > saturate > aromatic > asphaltene. Asphaltene consistently shows the lowest MSD values, indicating that the addition of the rejuvenator enhances the adhesion of aged asphaltene with aggregates. However, aged resin molecules still exhibit the worst adhesion with quartz, indicating that the rejuvenator primarily targets asphaltene rather than resin; this would explain why the adhesion of asphaltene to aggregate in practical situations is critical to the overall stability of an asphalt mixture [45].

At the calcite interface, the MSD values of the asphalt resins in the virgin samples are higher than those of the saturates, indicating that alkaline aggregates attract resins less than acidic aggregates. The MSD value rankings in Figure 11b–d are consistent with those in the corresponding quartz interfaces, suggesting that mineral acidity does not significantly affect the attraction order of aggregates to asphalt fractions. The diffusion coefficients of the different asphalts at various interfaces were calculated according to Equation (5) to quantitatively analyze the effect of aggregate acidity and alkalinity on the attraction of each asphalt component. A higher diffusion coefficient (D) indicates worse adhesion. The cohesion coefficient (Coh) is used to characterize the bonding strength between each component and aggregate, as calculated by Equation (6).

$$Coh = \frac{1}{D} \tag{6}$$

The results of Coh calculations for each component of asphalt at different interfaces are shown in Figure 13.

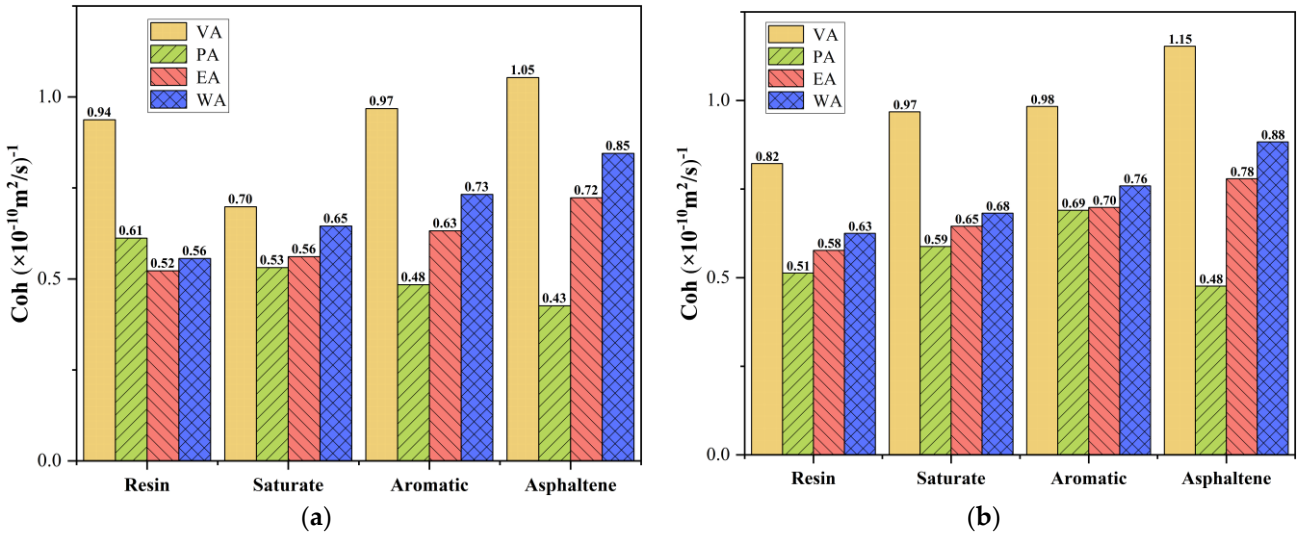

Figure 13. Calculated cohesion coefficients of asphalt components at different interfaces. (**a**) Quartz; (**b**) calcite.

In Figure 13, it is evident that the bonding properties of asphalt components with aggregates differ significantly, with asphaltene showing the largest difference. Therefore,

the cohesion coefficient of asphaltene was investigated. At the quartz interface, the cohesion coefficients of asphaltene in the aged asphalt, extracted oil-rejuvenated asphalt, and wood tar-rejuvenated asphalt were reduced by 59.5%, 31.3%, and 19.8%, respectively, compared with the virgin asphalt. Correspondingly, at the calcite interface, the cohesion coefficients were reduced by 58.7%, 32.4%, and 23.4%, respectively. The cohesion coefficient of asphaltene to aggregate in the aged asphalt was approximately 40% of that in the virgin asphalt, significantly increasing the likelihood of asphalt–aggregate detachment. The cohesion coefficients of the extracted oil-rejuvenated asphalt and wood tar-rejuvenated asphalt were about 70% and 80% of the virgin asphalt, respectively. These results are similar to the results of a study on the rejuvenation properties of actual wood tar [25], indicating that the addition of a rejuvenator effectively improves the cohesion between asphalt and aggregate. Moreover, the cohesion of asphaltene and aggregate in the wood tar-rejuvenated asphalt is superior to that in the extracted oil-rejuvenated asphalt. Additionally, the influence of aggregate acidity and alkalinity on asphaltene adhesion properties in different asphalts follows a similar trend, with alkaline aggregates exhibiting stronger attraction to asphalt than acidic aggregates. This can also be considered as a reason for the difference in the degree of bonding of realistic acid and alkaline aggregates with asphalt [46].

4.3. Analysis of the Interaction Energy between Asphalt and Aggregate

During the molecular simulation process, the conformational energy of the molecular system comprises both bonding and non-bonding energies. In the case of new and aged asphalt, which initially do not come into contact with each other, the main influencing factor of their interaction is the non-bonding energy ($E_{\text{potential}}$). This energy includes the van der Waals potential energy (E_{vdw}) and the electrostatic potential energy (E_e), which can be described using the Lennard–Jones function [32] and calculated as shown in Equations (7) and (8). As the aggregate remains stationary throughout the model, and its non-bonding energy is zero.

$$E_{vdw} = \sum_{i,j} \varepsilon_{ij} \left[2 \left(\frac{r_{ij}^0}{r_{ij}} \right)^9 - 3 \left(\frac{r_{ij}^0}{r_{ij}} \right)^6 \right] \tag{7}$$

$$E_e = \sum_{i,j} q_i q_j / 4\pi\varepsilon r_{ij} \tag{8}$$

where ε_{ij} is the energy parameter (kJ/mol); r_{ij} is the distance between atoms i and j (nm); r_{ij}^0 is the stabilizing distance between atoms i and j, i.e., the distance corresponding to the smallest potential energy (nm); q_i and q_j are the charges of atoms i and j, respectively (C); and ε is the dielectric constant (F/m).

E_{int} is the interaction energy between the asphalt and aggregate in different models, representing the energy required for individual systems to overcome intermolecular forces and merge into a single system. A higher E_{int} value indicates a stronger interaction between different molecules. The E_{int} value is calculated as shown in Equation (9). The interaction energy results between the asphalts and aggregates are illustrated in Figure 14.

$$E_{int} = E_{total} - E_A - E_B \tag{9}$$

where E_{total} is the potential energy of the asphalt mixing system (kJ/mol), and E_A and E_B are the potential energy of the aggregate and asphalt systems in the asphalt mixing system (kJ/mol), respectively.

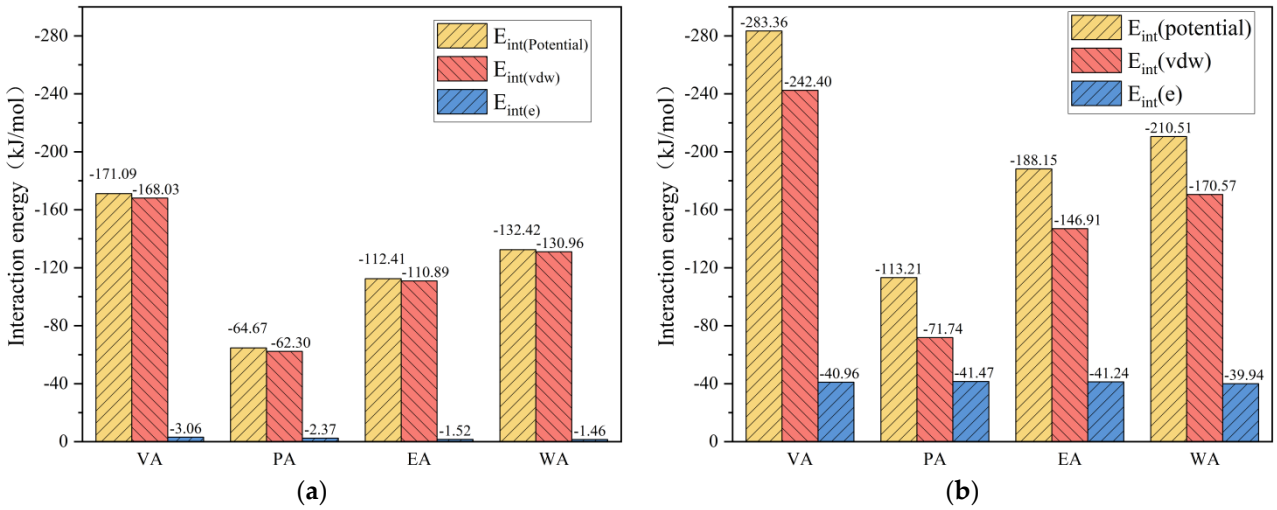

Figure 14. Interaction energy of asphalt in different aggregates. (**a**) Quartz; (**b**) calcite.

In Figure 14, it is evident that van der Waals potential energy plays a significant role in the interaction between asphalt and aggregate. The interaction energies are negative for both the acidic and alkaline aggregates, indicating an attractive force between asphalt and aggregate. The interaction energies of calcite with each asphalt are consistently higher than those of the corresponding quartz with each asphalt, suggesting a stronger bonding between calcite and asphalt. In addition, the E_e values in the calcite system are notably larger than those in the quartz system. This can be attributed to the presence of numerous calcium carbonate crystals in calcite, which generate suspended Ca^{2+} and CO_3^{2-} at the aggregate interface because of ionic bonding disruption during aggregate construction [44]. The generation of these ions increases the potential energy of the electrostatic force between asphalt and calcite. In contrast, silica primarily forms covalent bonds, and the exposed surfaces do not generate suspended ionic bonding. This further contributes to the disparity in energy interactions between asphalt and calcite compared with asphalt and quartz.

In the quartz system, the interaction energy values of the aged asphalt, extracted oil-rejuvenated asphalt, and wood tar-rejuvenated asphalt decreased by 62.2%, 34.3%, and 22.6%, respectively, compared with the virgin asphalt. The corresponding values in the calcite system were 60.0%, 33.6%, and 25.71%, respectively. These results indicate that the interaction energy between asphalt and both the acidic and alkaline aggregates follows a similar pattern, consistent with the aforementioned change in the cohesion coefficient. It can be observed that the magnitude of the interaction energy between asphalt and aggregate is positively correlated with the diffusion capacity of the asphalt molecules. The enhancement in interaction performance in the aged asphalt by the wood tar rejuvenator is significantly better than that of the extractive oil rejuvenator. This can be attributed to the wood tar rejuvenator's ability to improve the van der Waals potential energy (E_{vdw}) of the aged asphalt, indicating its effectiveness in enhancing the adhesion performance of aged asphalt with aggregates.

5. Effect of Moisture on the Interface Interactions between Asphalt and Aggregate

During the service life of asphalt pavements, moisture can have a detrimental impact. It can infiltrate the asphalt mixture, resulting in the formation of a three-phase asphalt–water–aggregate interfacial system. This, in turn, leads to a decrease in the mechanical and durability properties of the asphalt mixture. Traditional macroscopic experiments are unable to simulate the molecular-scale water damage phenomena in asphalt mixtures accurately. Therefore, molecular dynamics simulations were employed to investigate the effects of moisture on the interfaces of each material within the asphalt mixtures.

5.1. Construction of the Asphalt–Water–Aggregate Interface Model

A water layer with a density of 1.0 g/cm^3 and a thickness of 4 Å was created. The asphalt layer, water layer, and aggregate layer were stacked using the Build Layers module, with a vacuum layer of 60 Å added on top to avoid any adverse effects from the cyclic model generated by the three-dimensional periodic boundary conditions in the *Z*-axis direction. The aggregate remained fixed to minimize experimental errors. After constructing the model (shown in Figure 15), it was geometrically optimized to eliminate structural inconsistencies, and the NVT system was relaxed for 500 ps. All kinetic equilibria were performed at 298 K, with a time step of 1 fs and a truncation radius of 15.5 Å. Modeling proceeded with a time step of 1 fs.

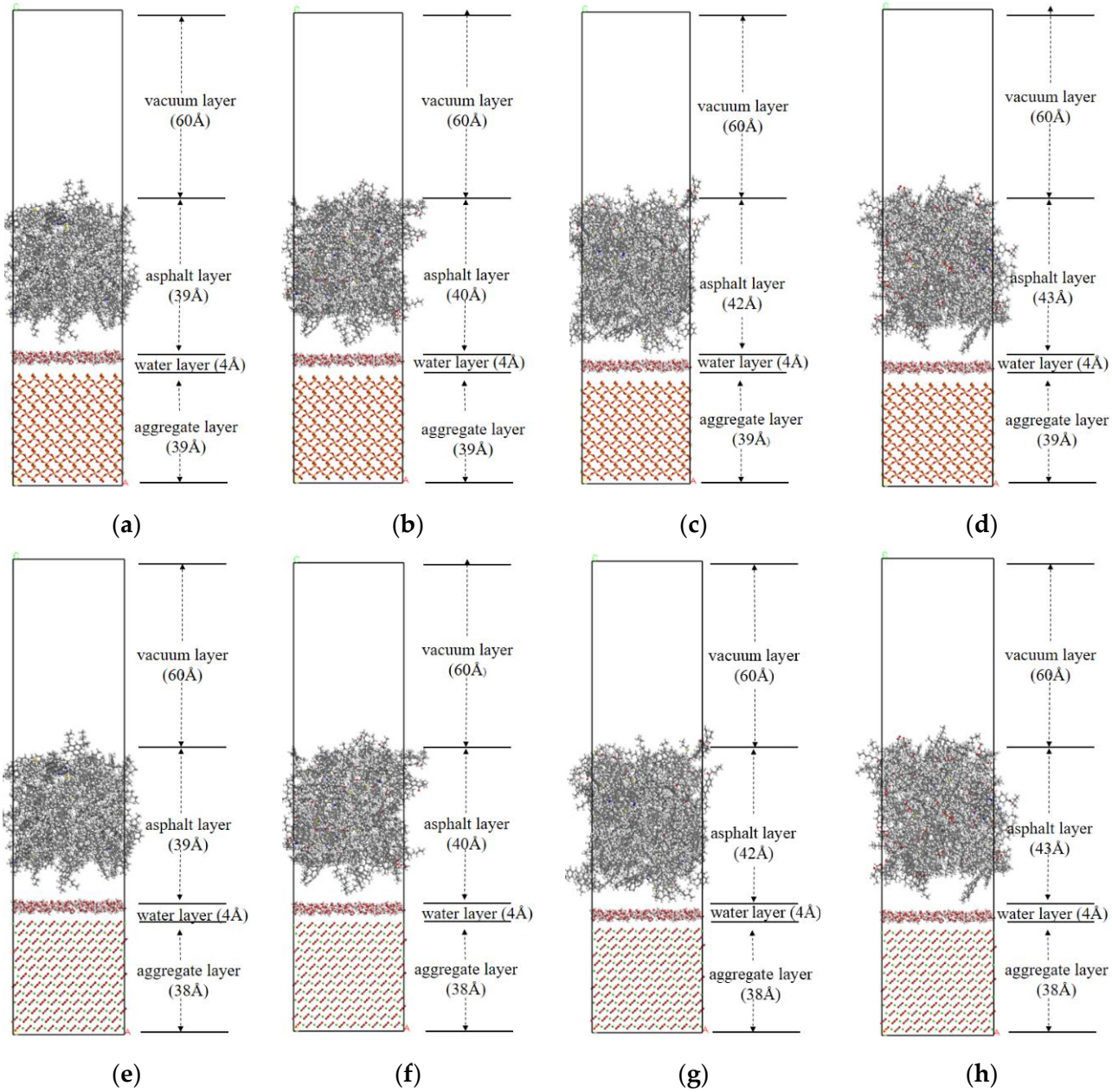

Figure 15. Model of the asphalt–water–aggregate interface. (**a**) VA–water–quartz; (**b**) PA–water–quartz; (**c**) EA–water–quartz; (**d**) WA–water–quartz; (**e**) VA–water–calcite; (**f**) PA–water–calcite; (**g**) EA–water–calcite; and (**h**) WA–water–calcite.

5.2. Diffusion Analysis of the Asphalt–Water–Aggregate Interface

To characterize the molecular aggregation of asphalt components under moisture intrusion, a radial distribution function (RDF) analytical model was employed. RDF represents the probability of other particles appearing within a distance (r) around a selected particle and is calculated as shown in Equation (10).

$$g(r) = \lim_{dr \to 0} \frac{dN/4\pi r^2 dr}{\rho} \tag{10}$$

where N is the number of specified atoms or groups at interval r from the reference atom or group; r is the distance of the specified atom or group from the reference atom or group (Å); and ρ is the bulk density of the whole system (g/cm^3).

For polymers, when g(r) = 1, it indicates that the molecules of each asphalt component are uniformly distributed. When g(r) > 1 or g(r) < 1, it indicates that the probability of other molecules appearing at that location is higher or lower, respectively, compared with a uniform distribution. Generally, a higher RDF value signifies a greater probability of molecular aggregation at a specific location. In this study, the RDF curves between each asphalt component and aggregate were analyzed in the asphalt–water–aggregate model at 298 K. The results are presented in Figures 16 and 17.

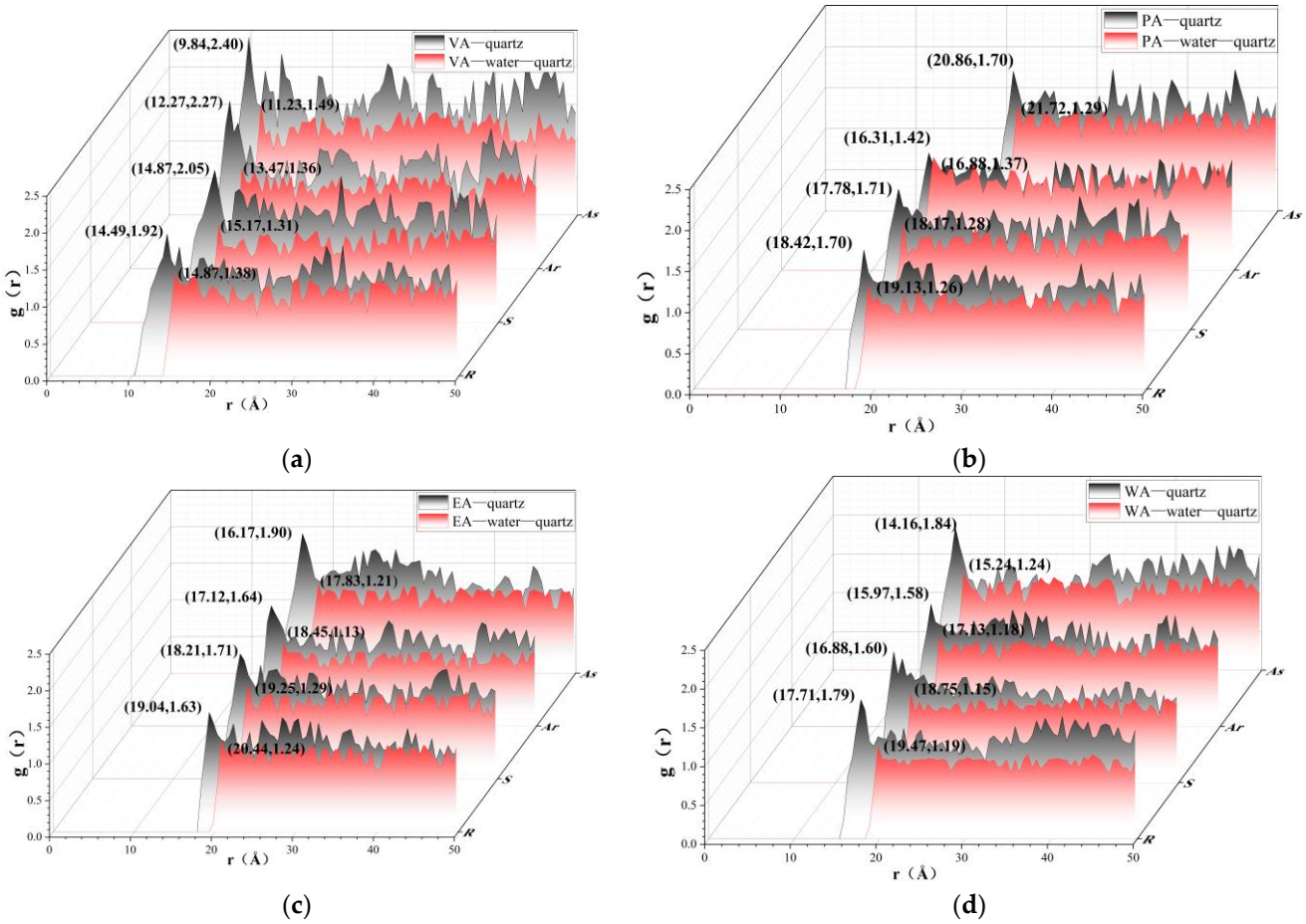

Figure 16. RDF curves of each asphalt with quartz under different humidity conditions. (**a**) VA–quartz; (**b**) PA–quartz; (**c**) EA–quartz; and (**d**) WA–quartz.

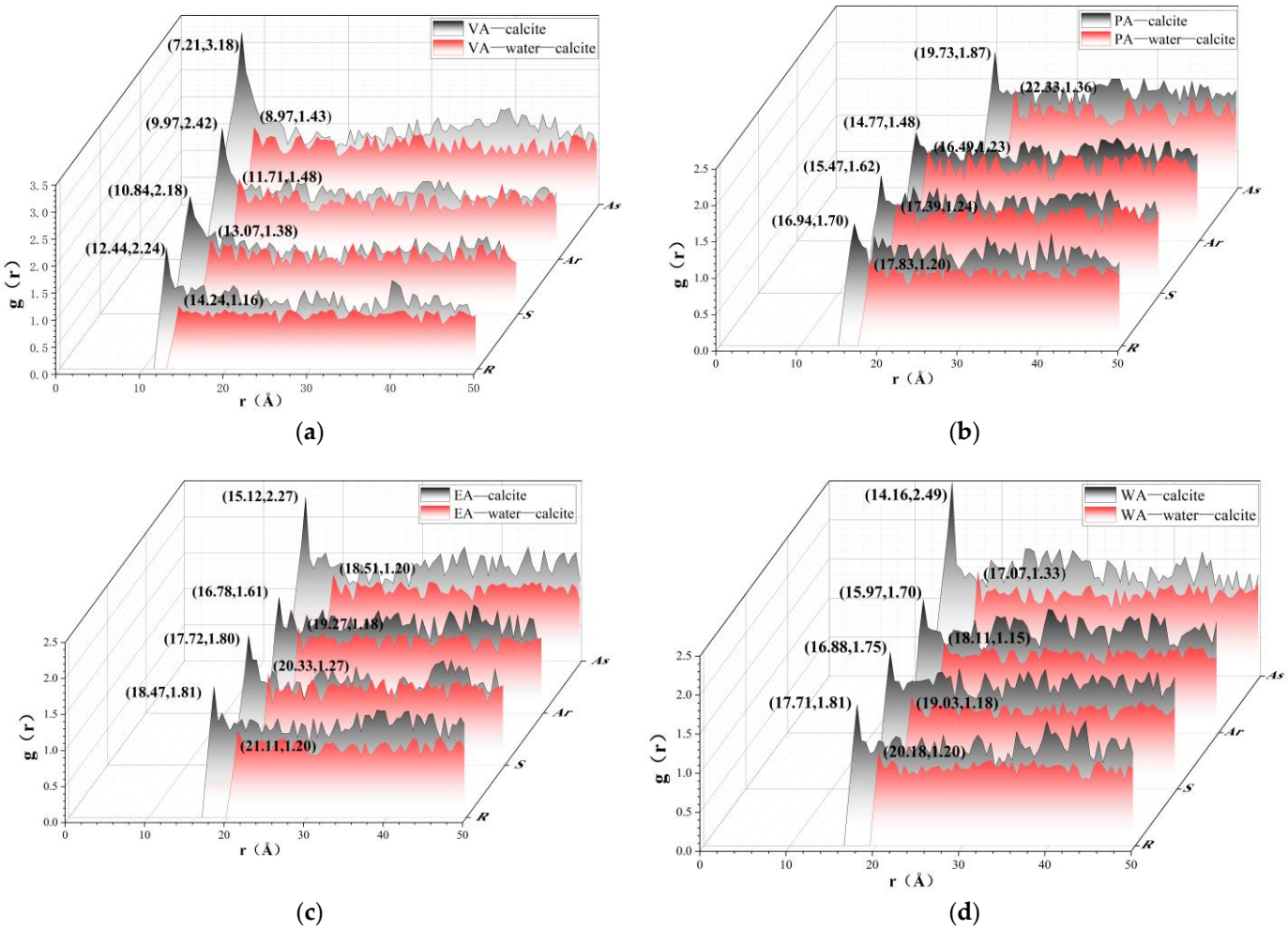

Figure 17. RDF curves of each asphalt with calcite under different humidity conditions. (**a**) VA–quartz; (**b**) PA–calcite; (**c**) EA–calcite; and (**d**) WA–calcite.

In the figure, it can be observed that the addition of moisture increases the distance between the aggregate and the components of the asphalt, regardless of whether the aggregate is acidic or basic. Additionally, the decreasing trend in the peak g(r) values of the asphalt components becomes more pronounced as the r-value increases, indicating that moisture reduces the degree of asphalt aggregation near the aggregate. The increase in the distance between asphalt and aggregate, combined with the decrease in aggregation, leads to the dislodging of aggregate and asphalt in the water-added asphalt mixture. Comparing Figures 15 and 16 reveals that the r-values and g(r) peaks of each component of the alkaline aggregate and asphalt in a dry environment are significantly higher than those of the corresponding acidic aggregate. This result confirms the earlier conclusion that the alkaline aggregate has a stronger attraction to asphalt and better adhesion performance than the acidic aggregate. In a wet environment, this pattern persists, although the peak g(r) values decrease significantly and no longer differ substantially from those of acidic aggregates. Most r-values of the alkaline aggregate with each asphalt component are still lower than those of the corresponding acidic aggregate, indicating that the degree of asphalt–aggregate aggregation in the alkaline aggregate system is more susceptible to water damage. However, the alkaline aggregate still exhibits better cohesion performance than acidic aggregate in a wet environment, which explains the difference in the water damage resistance of acid and alkaline aggregates at the molecular level [47].

In Figure 15, it is evident that the adhesion effect between each asphalt component and quartz in both dry and wet environments follows the order VA > WA > EA > PA,

with VA exhibiting the strongest adhesion and PA the weakest. The impact of moisture on the molecular aggregation of the asphalt components varies. As mentioned earlier, the adhesion effect between asphaltene and aggregate plays a crucial role. The largest effect of moisture can be observed on asphaltene, indicating that moisture primarily affects the adhesion effect of asphaltene. When transitioning from a dry to a wet environment, the peak g(r) value of asphaltene in the virgin asphalt decreases by 38.0%, and the r-value increases by 14.1%. For the aged asphalt, the peak g(r) value of asphaltene decreases by 24.0%, and the r-value increases by 4.1%. The extracted oil-asphalt experiences a decrease of 36.3% in the peak g(r) value of asphaltene, accompanied by an r-value increase of 10.3%. Similarly, the wood tar-rejuvenated asphalt shows a decrease of 32.6% in the peak g(r) value of asphaltene, with an r-value increase of 7.6%. Comparing these results, it can be concluded that the impact of moisture on asphaltene molecular aggregation follows the order VA > WA > EA > PA, with VA being the most affected and PA the least affected.

The alkaline aggregate system depicted in Figure 16 exhibits a similar pattern to the acidic aggregate system. In descending order, the r-values for each asphalt component in an acid/alkali environment are PA > EA > WA > VA. However, the impact of moisture on asphaltene molecular aggregation is the opposite of this order. Therefore, the effect of moisture intrusion on the adhesion effect between asphalt and aggregate is correlated with the distance (r). Moisture tends to weaken the adhesion capacity of asphalt closest to the aggregate, with the greatest reduction observed in the adhesion ability of the virgin asphalt at the closest distance from the aggregate. Conversely, the adhesion ability of the aged asphalt at the farthest distance from the aggregate shows the least reduction. Consequently, newly paved asphalt mixtures are initially more susceptible to water intrusion and asphalt aging damage. As the distance (r) increases, the influence of water intrusion gradually weakens, and the separation between asphalt and aggregate becomes dominated by asphalt aging. This can explain the fact that the aging of asphalt is more likely to cause detachment of the asphalt from the aggregate compared with moisture intrusion in practical situations [48].

Under both dry and wet environments, the distances between the peak g(r) points and the aggregate for each component of the virgin asphalt in the acidic environment were, in descending order, asphaltene (9.84 Å dry; 11.23 Å wet) < aromatic (12.27 Å dry; 13.47 Å wet) < colloidal (14.49 Å dry; 14.87 Å wet) < saturated (14.87 Å dry; 15.17 Å wet). This order remained consistent in the alkaline environment, indicating that asphaltenes and aromatics are more likely to aggregate on the aggregate surface in the virgin asphalt, and the sequence of these aggregated layers remained unchanged despite water intrusion. This pattern was also observed in other types of asphalt.

5.3. Analysis of the Interaction Energy of the Asphalt–Water–Aggregate Interface

The adhesion effect between asphalt and aggregate in the asphalt–water–aggregate interface model can also be characterized from an energy perspective. The interaction energy between the aggregate and asphalt is calculated using Equation (11) [23]. The results of non-bonding energy calculations for each system are presented in Tables 4 and 5, while the results of interaction energy calculations are depicted in Figure 17.

$$E_{\text{inter-agg}} = \left(E_{\text{aggw}} - E_{\text{aw}} - E_{\text{agw}} - E_{\text{a}} - E_{\text{ag}} + E_{\text{w}} + E_{\text{aag}}\right)/2 \quad (11)$$

where $E_{\text{inter-agg}}$ is the interaction energy between asphalt and aggregate (kJ/mol); E_{aggw} is the asphalt–water–aggregate system non-bonding energy (kJ/mol); E_{aw} is the asphalt and water layer of non-bonding energy (kJ/mol); E_{agw} is the aggregate and water layer of non-bonding energy (kJ/mol); E_{aag} is the asphalt and aggregate non-bonding energy (kJ/mol); and E_{a}, E_{ag}, and E_{w} are the asphalt, aggregate, and water layers of non-bonding energy (kJ/mol).

Table 4. Calculated non-bonding energy for each asphalt–water–quartz system (kJ/mol).

Asphalt Type	E_{aggw}	E_{aw}	E_{agw}	E_{aag}
VA	−6013.46	420.25	−5425.24	−1009.34
PA	−6417.37	621.55	−5422.52	−1417.69
EA	−5648.32	524.31	−5424.64	−1107.21
WA	−5877.54	427.79	−5424.73	−1180.34

Table 5. Calculated non-bonding energy for each bitumen–water–calcite system (kJ/mol).

Asphalt Type	E_{aggw}	E_{aw}	E_{agw}	E_{aag}
VA	−7141.76	430.77	−6638.24	−1109.28
PA	−7628.48	644.63	−6632.52	−1517.92
EA	−6842.75	527.83	−6634.64	−1207.75
WA	−6943.38	431.31	−6634.73	−1380.52

In Figure 18, it can be seen that the addition of water reduces the interaction energy between asphalt and aggregate. Compared with the dry environment, the interaction energies of VA, PA, EA, and WA in the acidic aggregate system under wet conditions decreased by 34.3%, 54.3%, 36.4%, and 24.7%, respectively. Therefore, from the perspective of interaction energy, the resistance to water damage of each asphalt ranks from strongest to weakest as WA > VA > EA > PA. The wood tar-rejuvenated asphalt demonstrated good resistance to water damage. As shown in Tables 4 and 5, this is because the wood tar rejuvenator improves the non-bonding energy between the aged asphalt and aggregate (E_{aag}) and contains aromatics with biomass alcohols that effectively reduce the non-bonding energy between asphalt and water (E_{aw}), thereby decreasing their mutual repulsion and further reducing the loss of interaction energy between asphalt and aggregate caused by water intrusion. In the alkaline aggregate system under wet conditions, the interaction energies of VA, PA, EA, and WA decreased by 41.9%, 62.2%, 30.4%, and 40.2%, respectively, compared with the dry environment. The ranking of each asphalt's ability to resist water damage from the energy perspective was the same as in the acidic aggregate system, but the decrease in energy for each asphalt in the alkaline aggregate system was greater than in the acidic aggregate system. As mentioned earlier, the contact area between alkaline aggregate and asphalt is larger than that of acidic aggregate under dry conditions, making it more difficult for moisture to penetrate the asphalt–aggregate interface. However, once moisture intrudes, the alkaline aggregate system is more susceptible to the adverse effects of moisture intrusion. This can explain the phenomenon that the water resistance of asphalt mixed with alkaline aggregate is better than that of asphalt mixed with acidic aggregate under the same conditions of practical application and, at the same time, it can explain the final small difference in the performance of the two aggregates after a long period of wetting environment [49].

To further quantitatively analyze the ability of each asphalt to resist water damage in different aggregate systems, the energy ratio (ER), defined as the ratio of adhesion work to stripping work, was used. Adhesion work refers to the energy required to bond asphalt and aggregate per unit area; a higher value indicates tighter bonding. Stripping work refers to the energy needed to displace water from the asphalt mixture per unit area. Because of the hydrophobic nature of asphalt and the hydrophilic nature of aggregates, stripping is a spontaneous process that does not require external energy; thus, lower stripping work means water replacement is less likely. Therefore, a larger ER value indicates stronger resistance to water damage. ER values are calculated as shown in Equations (12)–(14), and the results for each asphalt in different aggregate systems under wet conditions are presented in Figure 18.

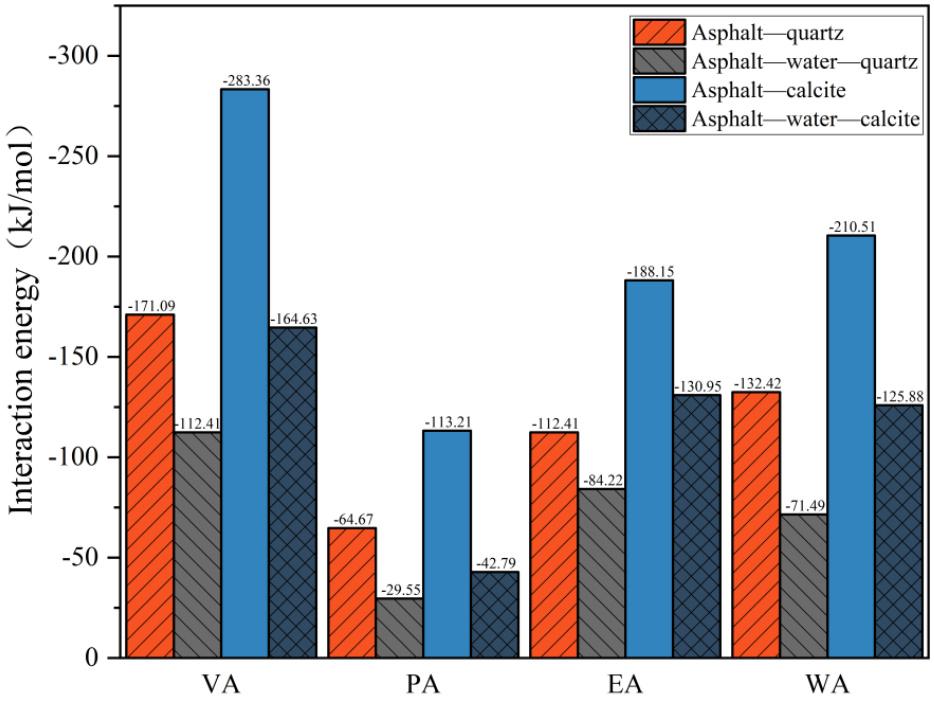

Figure 18. Interaction energy between asphalt and aggregate under dry/wet conditions.

$$W_{debonding} = \left(\Delta E_{inter\text{-}aw} + \Delta E_{inter\text{-}agw} - \Delta E_{inter\text{-}agg}\right)/A \quad (12)$$

$$W_{adhesion} = \Delta E_{inter\text{-}agg}/A \quad (13)$$

$$ER = \left|W_{adhesion}/W_{debonding}\right| \quad (14)$$

where $W_{debonding}$ is the stripping work (kJ/m^2); $W_{adhesion}$ is the adhesion work (kJ/m^2); $\Delta E_{inter\text{-}aw}$ is the interaction energy between asphalt and water (kJ/mol); $\Delta E_{inter\text{-}agw}$ is the interaction energy between aggregate and water (kJ/mol); $\Delta E_{inter\text{-}agg}$ is the interaction energy between asphalt and aggregate (kJ/mol); and A is the interfacial contact area between asphalt and aggregate (m^2).

In Figure 19, it is evident that the ER of asphalt in the alkaline aggregate system was higher than that in the acidic aggregate system. The ER values for each asphalt, in descending order, were WA > VA > EA > PA. Notably, the wood tar-rejuvenated asphalt exhibited enhanced resistance to water damage compared with the as-is asphalt. When compared with the aged asphalt, the wood tar-based rejuvenated asphalt and extracted oil-rejuvenated asphalt showed improvements of 78.2% and 43.5% in the acidic aggregate system and 98.1% and 44.4% in the alkaline aggregate system, respectively. This indicates that wood tar rejuvenators can significantly enhance the water damage resistance of aged asphalt. Furthermore, the wood tar rejuvenator in the alkaline aggregate system demonstrated a better improvement in water damage resistance for the aged asphalt compared with the acidic aggregate system.

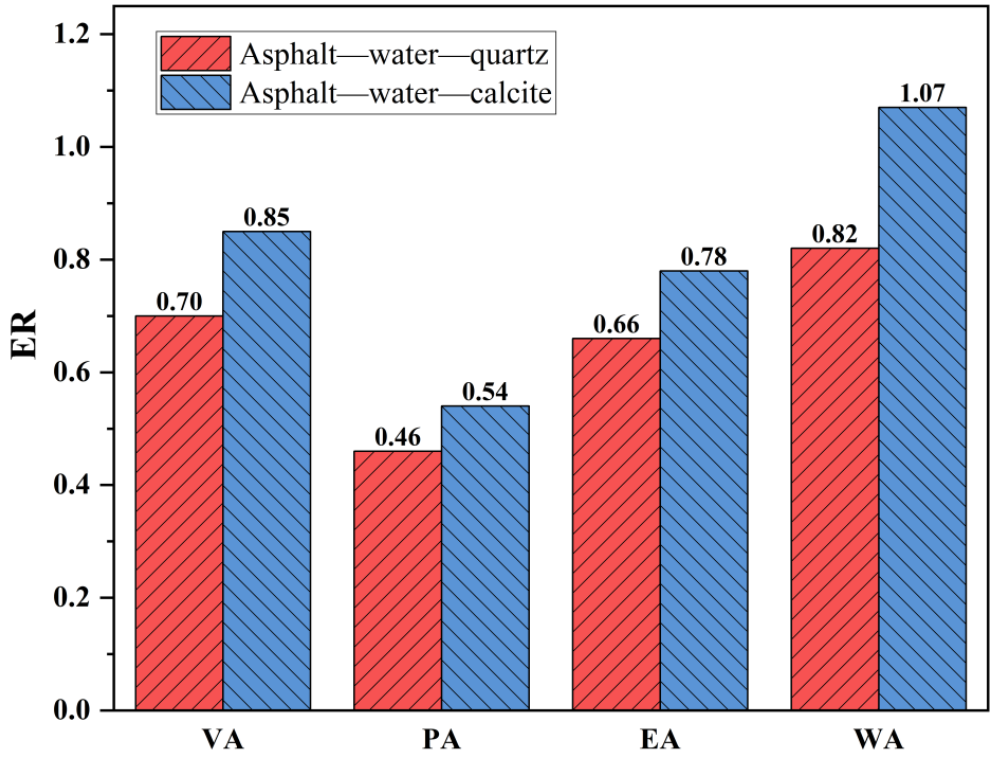

Figure 19. ER of each asphalt in various aggregate systems under different humid conditions.

6. Conclusions

In this study, the molecular dynamics simulation software Material Studio was utilized to simulate the mutual adhesion process between wood tar-rejuvenated asphalt and aggregates, representing both acidic and alkaline environments under dry and wet conditions. The aim was to evaluate the adhesion effect of wood tar-rejuvenated asphalt using relevant indices and investigate the role of wood tar rejuvenators in improving the adhesion effect between aged asphalt and aggregates. Ultimately, this study sought to elucidate the mechanism by which rejuvenated asphalt enhances resistance to water damage. The main findings are as follows:

(1) Wood tar-rejuvenated asphalt exhibits favorable adhesion properties to both acidic and alkaline aggregates under dry conditions. The incorporation of a wood tar rejuvenator enhances the interaction energy between aged asphalt and aggregate, thereby intensifying the mutual attraction between the two and expanding the contact area. The adhesion between asphalt and aggregate primarily relies on the adhesion effect between asphaltene and aggregate. Wood tar plays a crucial role in stabilizing the aggregation of asphaltene near the aggregate by reducing its diffusion capability in the presence of attractive forces from the aggregate.

(2) The intrusion of moisture diminishes the adhesion between asphalt and aggregate. As the presence of water increases, the aggregation distance between these materials and reduces their degree of aggregation, thereby weakening the interaction between asphalt and aggregate. The extent of water damage is correlated with the aggregation distance between asphalt and aggregate; a greater distance corresponds to more significant damage, and vice versa.

(3) Under wet conditions, wood tar-rejuvenated asphalt demonstrates the ability to enhance the adhesion function between aged asphalt and aggregate while simultaneously reducing the stripping function induced by water replacement. Consequently, it exhibits superior resistance to water damage compared with conventional asphalt.

(4) Under humid conditions, the aromatics in wood tar, which possess biomass–alcoholic properties, can effectively diminish the mutual repulsion between asphalt and water,

thereby alleviating the loss of interaction energy between asphalt and aggregate caused by water intrusion. Consequently, wood tar-rejuvenated asphalt outperforms extracted oil-rejuvenated asphalt in terms of resistance to water damage.

(5) Under dry conditions, the adhesion of bitumen to the basic aggregate was found to be stronger compared with the acidic aggregate. However, under wet conditions, the bitumen–basic aggregate system exhibited increased susceptibility to water damage. Nonetheless, it still demonstrated overall superior adhesion when compared with the acidic aggregate system.

(6) This study provides new judging criteria for the selection of rejuvenators for waste asphalt, which can help in the future selection of superior rejuvenators for rejuvenating aged asphalt and reduce the possibility of selecting the wrong rejuvenator for future follow-up experiments. Meanwhile, this study supports the possibility and suitability of using wood tar as a rejuvenator from the molecular dynamics point of view. The results can provide a theoretical basis for biomass material-based rejuvenators at the practical application level and contribute to the management of environmental pollution caused by waste asphalt around the world.

(7) Currently, all asphalt models used for MD simulation are representative models. There is still a large gap between these models and actual asphalt, which makes MD simulation have unavoidable errors from the source. In future studies, with the advancement of computer and simulation science, it is necessary to improve simulation accuracy and conduct multi-scale simulations to obtain more accurate simulation and calculation results.

Author Contributions: Conceptualization, K.L. and Q.L.; methodology, L.X.; validation, G.G. and D.Z.; formal analysis, L.X.; investigation, Y.L.; resources, X.C.; data curation, G.G.; writing—original draft preparation, L.X.; writing—review and editing, K.L. All authors have read and agreed to the published version of the manuscript.

Funding: This work was supported by the Key Research and Development Program of Hunan Province, China [Grant No. 2023SK2078] and the Graduate Innovation Fund of the Central South University of Forestry and Technology, China.

Institutional Review Board Statement: Not applicable.

Informed Consent Statement: Not applicable.

Data Availability Statement: Data is contained within the article.

Conflicts of Interest: Xing Chen was employed by the company Hunan Expressway Engineering Consulting Co., Ltd. The remaining authors declare that the research was conducted in the absence of any commercial or financial relationships that could be construed as a potential conflict of interest. The brand names mentioned in this paper are for the reader's convenience only and do not suggest any endorsement by the authors.

References

1. Joumblat, R.; Kassem, H.; Elkordi, A.; Khatib, J. Use of alternative recycled fillers in bituminous mixtures: A review. *Adv. Upcycling By-Prod. Bind. Bind.-Based Mater.* **2024**, 335–356.
2. Zou, F.; Wu, M.M.; Tan, Z.; Lu, G.; Kwok, K.W.; Leng, Z. Ecotoxicological risk of asphalt pavements to aquatic animals associated with pollutant leaching. *Sci. Total Environ.* **2024**, *944*, 173985. [CrossRef] [PubMed]
3. Wang, W.; Wang, L.; Xiong, H.; Luo, R. A review and perspective for research on moisture damage in asphalt pavement induced by dynamic pore water pressure. *Constr. Build. Mater.* **2019**, *204*, 631–642. [CrossRef]
4. Huang, G.; Zhang, J.; Wang, Z.; Guo, F.; Li, Y.; Wang, L.; He, Y.; Xu, Z.; Huang, X. Evaluation of asphalt-aggregate adhesive property and its correlation with the interaction behavior. *Constr. Build. Mater.* **2023**, *374*, 130909. [CrossRef]
5. Li, C.; Xiao, M.; Dong, J.; Ren, J.; Guo, X. Study on the factors affecting the self-healing performance of asphalt mixture and pavement based on fracture mechanics and calculation formula. *Theor. Appl. Fract. Mech.* **2023**, *126*, 103954. [CrossRef]
6. Bagampadde, U.; Isacsson, U.; Kiggundu, B.M. Classical and contemporary aspects of stripping in bituminous mixes. *Road Mater. Pavement Des.* **2004**, *5*, 7–43. [CrossRef]
7. Yalghouzaghaj, M.N.; Sarkar, A.; Hamedi, G.H.; Hayati, P. Application of the surface free energy method on the mechanism of low-temperature cracking of asphalt mixtures. *Constr. Build. Mater.* **2021**, *268*, 121194. [CrossRef]

8. Sun, Z.; Qi, H.; Li, S.; Tan, Y.; Yue, Z.; Lv, H. Estimating the effect of coarse aggregate meso-structure on the thermal contraction of asphalt mixture by a hierarchical prediction approach. *Constr. Build. Mater.* **2022**, *342*, 128048. [CrossRef]
9. Poulikakos, L.D.; Partl, M.N. Investigation of porous asphalt microstructure using optical and electron microscopy. *J. Microsc.* **2010**, *240*, 145–154. [CrossRef]
10. Wang, L.; Li, Q.; Liu, K.; Jiang, K. Fatigue performance analysis and life prediction of wood tar rejuvenated asphalt. *Int. J. Pavement Res. Technol.* **2023**, 1–12. [CrossRef]
11. Bhasin, A.; Izadi, A.; Bedgaker, S. Three dimensional distribution of the mastic in asphalt composites. *Constr. Build. Mater.* **2011**, *25*, 4079–4087. [CrossRef]
12. Guo, M.; Tan, Y.; Yu, J.; Hou, Y.; Wang, L. A direct characterization of interfacial interaction between asphalt binder and mineral fillers by atomic force microscopy. *Mater. Struct.* **2017**, *50*, 141. [CrossRef]
13. Mo, L.; Huurman, M.; Wu, S.; Molenaar, A.A.A. Ravelling investigation of porous asphalt concrete based on fatigue characteristics of bitumen–stone adhesion and mortar. *Mater. Des.* **2009**, *30*, 170–179. [CrossRef]
14. Wu, H.; Ji, X.; Song, W.; Deng, Z.; Zhan, Y.; Zou, X.; He, F. Multi-scale analysis on fracture behaviors of asphalt mixture considering moisture damage. *Constr. Build. Mater.* **2024**, *416*, 135234. [CrossRef]
15. Zou, Y.; Gao, Y.; Chen, A.; Wu, S.; Li, Y.; Xu, H.; Amirkhanian, S. Adhesion failure mechanism of asphalt-aggregate interface under an extreme saline environment: A molecular dynamics study. *Appl. Surf. Sci.* **2024**, *645*, 158851. [CrossRef]
16. Joumblat, R.; Kassem, H.A.; Al Basiouni Al Masri, Z.; Elkordi, A.; Al-Khateeb, G.; Absi, J. Performance evaluation of hot-mix asphalt with municipal solid waste incineration fly ash using the stress sweep rutting test. *Innov. Infrastruct. Solut.* **2023**, *8*, 261. [CrossRef]
17. Wong TL, X.; Hasan MR, M.; Peng, L.C. Recent development, utilization, treatment and performance of solid wastes additives in asphaltic concrete worldwide: A review. *J. Traffic Transp. Eng. (Engl. Ed.)* **2022**, *9*, 693–724. [CrossRef]
18. Li, J.; Qin, Y.; Zhang, X.; Shan, B.; Liu, C. Emission Characteristics, Environmental Impacts, and Health Risks of Volatile Organic Compounds from Asphalt Materials: A State-of-the-Art Review. *Energy Fuels* **2024**, *38*, 4787–4802. [CrossRef]
19. Liu, K.; Liu, C.; Li, Q.; Jiang, K. Laboratory investigation of the low-temperature crack resistance of wood tar-based rejuvenated asphalt mixture based on the semi-circular bend and trabecular bending test. *Materials* **2022**, *15*, 7223. [CrossRef]
20. Li, S.; Wang, F.; Ouyang, L.; Chen, X.; Yang, Z.; Rozga, P.; Fofana, I. Differential low-temperature AC breakdown between synthetic ester and mineral oils: Insights from both molecular dynamics and quantum mechanics. *IEEE Trans. Dielectr. Electr. Insul.* **2023**, *38*, 4787–4802. [CrossRef]
21. Sun, B. Analysis of Thermal Properties of Rejuvenated Asphalt Using Molecular Dynamic Simulations. In Proceedings of the 17th COTA International Conference of Transportation Professionals, Shanghai, China, 7–9 July 2017; American Society of Civil Engineers: Reston, VA, USA, 2017; pp. 2924–2931.
22. Xu, G.; Wang, H. Molecular dynamics study of oxidative aging effect on asphalt binder properties. *Fuel* **2017**, *188*, 1–10. [CrossRef]
23. Yao, H.; Dai, Q.; You, Z. Chemo-physical analysis and molecular dynamics (MD) simulation of moisture susceptibility of nano hydrated lime modified asphalt mixtures. *Constr. Build. Mater.* **2015**, *101*, 536–547. [CrossRef]
24. Cui, B.; Wang, H. Molecular interaction of Asphalt-Aggregate interface modified by silane coupling agents at dry and wet conditions. *Appl. Surf. Sci.* **2022**, *572*, 151365. [CrossRef]
25. Yao, X.; Li, C.; Xu, T. Interfacial adhesive behaviors between SBS modified bitumen and aggregate using molecular dynamics simulation. *Surf. Interfaces* **2022**, *33*, 102245. [CrossRef]
26. Liu, J.; Yu, B.; Hong, Q. Molecular dynamics simulation of distribution and adhesion of asphalt components on steel slag. *Constr. Build. Mater.* **2020**, *255*, 119332. [CrossRef]
27. Gong, Y.; Xu, J.; Yan, E.H. Intrinsic temperature and moisture sensitive adhesion characters of asphalt-aggregate interface based on molecular dynamics simulations. *Constr. Build. Mater.* **2021**, *292*, 123462. [CrossRef]
28. Zheng, C.; Shan, C.; Liu, J.; Zhang, T.; Yang, X.; Lv, D. Microscopic adhesion properties of asphalt–mineral aggregate interface in cold area based on molecular simulation technology. *Constr. Build. Mater.* **2021**, *268*, 121151. [CrossRef]
29. Zhou, X.; Moghaddam, T.B.; Chen, M.; Wu, S.; Adhikari, S.; Wang, F.; Fan, Z. Nano-scale analysis of moisture diffusion in asphalt-aggregate interface using molecular simulations. *Constr. Build. Mater.* **2021**, *285*, 122962. [CrossRef]
30. Luo, L.; Chu, L.; Fwa, T.F. Molecular dynamics analysis of moisture effect on asphalt-aggregate adhesion considering anisotropic mineral surfaces. *Appl. Surf. Sci.* **2020**, *527*, 146830. [CrossRef]
31. Su, M.; Zhang, H.; Zhang, Y. Miscibility mechanical properties of SBS and asphalt blends based on molecular dynamics simulation. *J. Chang. Univ. (Nat. Sci. Ed.)* **2017**, *37*, 24–32.
32. Yao, H.; Liu, J.; Xu, M.; Ji, J.; Dai, Q.; You, Z. Discussion on molecular dynamics (MD) simulations of the asphalt materials. *Adv. Colloid Interface Sci.* **2022**, *299*, 102565. [CrossRef] [PubMed]
33. Ding, H.; Wang, H.; Qu, X.; Varveri, A.; Gao, J.; You, Z. Towards an understanding of diffusion mechanism of bio-rejuvenators in aged asphalt binder through molecular dynamics simulation. *J. Clean. Prod.* **2021**, *299*, 126927. [CrossRef]
34. Zheng, W.; Wang, H.; Chen, Y.; Ji, J.; You, Z.; Zhang, Y. A review on compatibility between crumb rubber and asphalt binder. *Constr. Build. Mater.* **2021**, *297*, 123820. [CrossRef]
35. Le Guern, M.; Chailleux, E.; Farcas, F.; Dreessen, S.; Mabille, I. Physico-chemical analysis of five hard bitumens: Identification of chemical species and molecular organization before and after artificial aging. *Fuel* **2010**, *89*, 3330–3339. [CrossRef]

36. Guo, M.; Liang, M.; Fu, Y.; Sreeram, A.; Bhasin, A. Average molecular structure models of unaged asphalt binder fractions. *Mater. Struct.* **2021**, *54*, 173. [CrossRef]
37. Ren, S.; Liu, X.; Lin, P.; Erkens, S.; Xiao, Y. Chemo-physical characterization and molecular dynamics simulation of long-term aging behaviors of bitumen. *Constr. Build. Mater.* **2021**, *302*, 124437. [CrossRef]
38. *JTG E20-2011*; Test Procedure for Bitumen and Bitumen Mixture for Highway Engineering. Ministry of Transport of the People's Republic of China: Beijing, China, 2011.
39. Li, Y.; Ling, H. Comparative study on capillary gas chromatographic analysis of organic components of wood vineger and water-extract of wood-tar prepared from hard wood barks. *J. Anal. Sci.* **2017**, *28*, 58–62.
40. Fagernäs, L.; Kuoppala, E.; Tiilikkala, K.; Oasmaa, A. Chemical composition of birch wood slow pyrolysis products. *Energy Fuels* **2012**, *26*, 1275–1283. [CrossRef]
41. McKenna, A.M.; Donald, L.J.; Fitzsimmons, J.E.; Juyal, P.; Spicer, V.; Standing, K.G.; Marshall, A.G.; Rodgers, R.P. Heavy petroleum composition. 3. Asphaltene aggregation. *Energy Fuels* **2013**, *27*, 1246–1256. [CrossRef]
42. Zhang, Y.; Yao, K.; Zhi, P.; Dong, Y.; Feng, X.; Li, B.; Xu, Y.; Zhang, Y.; Guo, C.; Tian, J. The influence of water acidity and alkalinity on the adhesion properties of bitumen-aggregate interface. *Colloids Surf. A Physicochem. Eng. Asp.* **2024**, *695*, 134025. [CrossRef]
43. Guo, M.; Yin, X.; Du, X.; Tan, Y. Effect of aging, testing temperature and relative humidity on adhesion between asphalt binder and mineral aggregate. *Constr. Build. Mater.* **2023**, *363*, 129775. [CrossRef]
44. Lin, J. Molecular Dynamics Study of Diffusion Behavior of Virgin and Recycled Asphalt Binder. Master Dissertation, Southeast University, Nanjing, China, 2019.
45. Salehzadeh, M.; Husein, M.M.; Ghotbi, C.; Taghikhani, V.; Dabir, B. Investigating the role of asphaltenes structure on their aggregation and adsorption/deposition behavior. *Geoenergy Sci. Eng.* **2023**, *230*, 212204. [CrossRef]
46. Zhang, Y.; Xu, Y.; Yao, K.; Zhang, Y.; Wei, Y.; Feng, X.; Wei, X. Evaluation of Asphalt-Aggregate Interfacial Adhesion in Different Acid-Base Solutions Based on Dlvo Theory. *SSRN* **2023**. [CrossRef]
47. Raghunathan, V.; Ayyappan, V.; Dhilip, J.D.J.; Sundarrajan, D.; Rangappa, S.M.; Siengchin, S. Influence of alkali-treated and raw *Zanthoxylum acanthopodium* fibers on the mechanical, water resistance, and morphological behavior of polymeric composites for lightweight applications. *Biomass Convers. Biorefinery* **2023**, 1–13. [CrossRef]
48. Yang, B.; Li, H.; Sun, Y.; Zhang, H.; Liu, J.; Yang, J.; Zhang, X. Chemo-rheological, mechanical, morphology evolution and environmental impact of aged asphalt binder coupling thermal oxidation, ultraviolet radiation and water. *J. Clean. Prod.* **2023**, *388*, 135866. [CrossRef]
49. Zhang, D.; Xu, P.; Yu, P.; Hu, Q.; Luan, D. Influence of Acidity and Alkalinity of Water Environment on Water Stability of Asphalt Mixture: Phase II-Microscopic Erosion Mechanism. *Int. J. Adhes. Adhes.* **2024**, *132*, 103738. [CrossRef]